IEEE Access
Multidisciplinary | Rapid Review | Open Access Journal

Received 1 May 2023, accepted 15 May 2023, date of publication 17 May 2023, date of current version 9 June 2023.

Digital Object Identifier 10.1109/ACCESS.2023.3277202

RESEARCH ARTICLE

Improvement of Frequency Regulation of a Wind-Integrated Power System Based on a PD-PIDA Controlled STATCOM Tuned by the Artificial Rabbits Optimizer

NABEEL MOHAMMED NEAMAH[1], AHMED ABUHUSSEIN[2], (Member, IEEE), AHMED A. HOSSAM-ELDIN[3], (Life Senior Member, IEEE), SULTAN ALGHAMDI[4,5], (Member, IEEE), AND KAREEM M. ABORAS[3]

[1]Department of Power and Electrical Machines, College of Engineering, University of Diyala, Baqubah 32008, Iraq
[2]Department of Electrical and Cyber Engineering, Gannon University, Erie, PA 16541, USA
[3]Department of Electrical Power and Machines, Faculty of Engineering, Alexandria University, Alexandria 21544, Egypt
[4]Smart Grids Research Group, Center of Research Excellence in Renewable Energy and Power Systems, King Abdulaziz University, Jeddah 21589, Saudi Arabia
[5]Department of Electrical and Computer Engineering, Faculty of Engineering, King Abdulaziz University, Jeddah 21589, Saudi Arabia

Corresponding author: Kareem M. AboRas (kareem.aboras@alexu.edu.eg)

ABSTRACT In this research, a novel optimized Proportional-Derivative with Proportional-Integral-Derivative-Acceleration (PD-PIDA) driven static synchronous compensator (STATCOM) is proposed with the goal of improving the frequency performance of power systems through the manipulation of reactive power. When there is a variation in load or when there is a failure of generation, the presented controller is able to maintain the frequency of the system within the allowable limits (±2% as per IEC 60034–1 standard). A recently developed metaheuristic optimization strategy known as the Artificial Rabbits Optimizer, or ARO, is used to do the fine-tuning the PD-PIDA controller's gain settings. In addition to this, the functionality of the ARO-based PD-PIDA-controlled STATCOM is evaluated in the context of two IEEE standard systems: the two-area four-machine system (Kundur system) and the New England IEEE 39-bus system. According to the outcomes, the ARO-based PD-PIDA controller can give a superior frequency response than the PIDA controller whose parameters are optimized by Marine Predator Algorithm (MPA) that was published in the prior literature. This was determined by comparing the two controllers. In addition, the proposed controller's resiliency is tested by integrating case studies with wind generation. This helps to ensure that the controller is fit for purpose. In every single one of the examples that were researched, the application of the ARO-based PD-PIDA-controlled STATCOM resulted in a remarkable boost in the frequency performance. Additionally, the outputs are introduced in the form of time domain simulations that were carried out with MATLAB/SIMULINK.

INDEX TERMS STATCOM, ARO, PD controller, PIDA controller, frequency regulation, Kundur system, IEEE 39 bus system.

NOMENCLATURE

PD	Proportional-Derivative.
PI	Proportional-Integral.
PID	Proportional-Integral-Derivative.
PIDA	Proportional-Integral-Derivative-Acceleration.
PD-PIDA	Proportional-Derivative with Proportional-Integral-Derivative-Acceleration.
ARO	Artificial Rabbits Optimizer.
MPA	Marine Predator Algorithm.
DTBO	Driving Training-Based Optimization.
PV	Photovoltaic.

The associate editor coordinating the review of this manuscript and approving it for publication was Mostafa M. Fouda.

STATCOM	Static synchronous compensator.
PLL	Phase Locked Loop.
PWM	Pulse Width Modulation.
LFC	Load Frequency Control.
VSC	Voltage Source Converter.
RESs	Renewable Energy Sources.
ObjFn	Objective Function.
Max. O.	Maximum Overshoot (Hz).
Max. U.	Maximum Undershoot (Hz).
St. St. Frequency	Steady State Frequency (Hz).
St. St. Q	Steady State STATCOM reactive power (Mvar).
KP_{PD}	Proportional action of the PD controller.
KD_{PD}	Derivative action of the PD controller.
NF_{PD}	Derivative action filter coefficient of the PD controller.
KP_{PIDA}	Proportional action of the PIDA controller.
KI_{PIDA}	Integral action of the PIDA controller.
$KD1_{PIDA}$	First derivative action of the PIDA controller.
$KD2_{PIDA}$	Second derivative action of the PIDA controller.
NF1	First derivative action filter coefficient of the PIDA controller.
NF2	Second derivative action filter coefficient of the PIDA controller.
ESS	Energy Storage Systems.

I. INTRODUCTION

A. BACKGROUND AND LITERATURE REVIEW

Frequency stability, voltage management, and active power oscillations are only some of the dynamic stability difficulties that modern power systems must contend with [1], [2]. There are a number of factors that contribute to the degradation of system frequency stability, including the lack of system inertia brought on by the rising growth of renewable energy sources (RESs), unexpected load disruption, and failure of a generation unit [3], [4]. Consequently, if the system is exposed to unbalance between generation and load, it is essential to maintain the system frequency within the allowable variation boundaries of its normal value [5]. In situations when a loss of generation causes a drop in frequency and a rapid decrease in load causes a rise in frequency [6]. Both can result in the withdrawal of some generating sources by over-frequency or under-frequency protection mechanisms, which in turn causes inadequate functioning of the power system, which can result in a blackout of the system [7], [8].

Figure. 1 depicts the performance of frequency in a power system after the disconnection of a generation unit [9]. The frequency will start declining at a rapid pace from P1 to P3, based on the inertia of the power system and severity of the disturbances, with P3 named as the frequency nadir, or the lowest frequency value attained for the transient duration. Furthermore, as shown in Figure. 1, the frequency difference between P1 and P3 defines the maximum undershoot of the frequency. Finally, the frequency begins to retrace to P2 (the settling or steady state frequency). In order to keep the frequency within the allowed constraints, the average power balance that exists between the generator and the load has to be regained as soon as possible [10].

The frequency stability of power systems has been the focus of research and development over the course of the last several decades, which has led to the development of a number of different control strategies. For instance, traditional methods like as spinning reserve allocation [11], [12] and load shedding [13], [14] have been established for the scenario of an under-frequency issue. In situations when spinning reserve allocation is used, certain producing units have their loads reduced so that they can respond appropriately to any unforeseen drop in output caused by the governors that control them [11], [12]. In addition, if generators are unable to offer additional real power in a timely manner, then load shedding is the most expedient way to boost the frequency performance of the power system [13], [14]. Although, in the event of an over-frequency issue, some studies have proposed enhancing the governor reaction by incorporating a supplementary governor-based power system stabilizer (auxiliary governor) [15], [16]. Also, controlled generation trips would be the sole option if the preceding control mechanism wasn't quick enough [17].

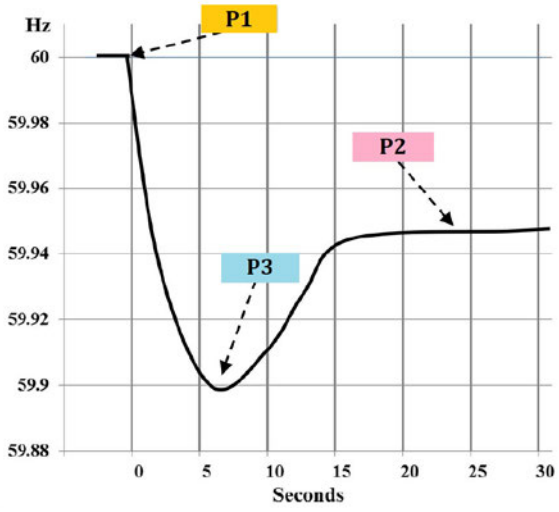

FIGURE 1. The power system's frequency performance under the effect of generation failure [9].

In addition, several load frequency controllers (LFCs) have been recommended for use in power grids and microgrids in order to maintain the acceptable limits for the frequency variations and the tie-line power variations. Classical proportional-integral-derivative (PID) regulators have been employed for LFCs; for instance, the regulators given in [18], [19], and [20] utilise various optimization strategies in order to optimise the system frequency performance

to various disturbances. Additionally, fuzzy PID-LFCs with a variety of recommended methodologies have been presented in [21], [22], and [23] to regulate the frequency of microgrid multi-source and multiarea systems. Introducing virtual inertia into a system is one more strategy that has been proposed to boost the frequency performance of low-inertia systems [24], [25]. Increased system inertia [26] is achieved by careful regulation of the converters of renewable energy sources (RESs) and energy storage systems (ESS).

The previously discussed strategies all share a dependency on active power regulation as a crucial pillar with the implicit premise that the active power-frequency channel and the reactive power-voltage channel are unrelated. Nevertheless, these two channels interact in a way that is not immediately obvious, and this interaction provides an extra possibility for enhancing the primary frequency response. This type of indirect influence was also discussed in [27]. To make the presentation of a straightforward power system state-space model easier, the author chose to ignore the coefficients that existed between $\Delta\omega_r$ (rotor angular velocity variation), $\Delta\delta$ (rotor angular position variation), and ΔV_f (exciter voltage variation). According to the outcomes presented in [28], eliminating the global power imbalance is equivalent to dampening the common frequency mode. This fact led the authors of [29] to present a synchronous condenser relies on a Multi-Band Controller (MBC) as a means of controlling low-frequency fluctuations via the voltage channel. This allows them to build a novel control scheme for increasing primary frequency responsiveness by using the influence of voltage on extremely low frequency dynamics.

In addition, renewable power sources with inverter control, particularly photovoltaic (PV) units, have lately been employed to deliver reactive power for load frequency and voltage stability as well as power deviation control [30]. In addition, converter management of energy storage units are used for the purpose of improving frequency control inside microgrids [31], [32], [33]. Rather than relying just on active power, as is done in more conventional approaches, this method may also take use of VAR manipulation for the purpose of frequency control. In the study referenced by [34], non-critical loads had a series compensator attached to them in order to produce a smart load design. This configuration has the ability to increase the frequency response by applying VAR modulation. In addition, the authors of [35] have presented a controller based STATCOM as a means of further improving the frequency performance of a wind farm integrated power system. They suggested the use of the well-known PIDA controller, which has been shown to be effective in a large number of published research due to its capacity to improve the dynamic characteristics of systems due to the fact that, in comparison to a traditional PID controller it can provide two extra zeros to its formula. For the purpose of fine-tuning the PIDA controller gains, the Marine Predator Algorithm (MPA) is utilised.

B. MOTIVATION AND CONTRIBUTIONS

Encouraged by their success, the authors continued along this path, proposing the PD-PIDA controller, which has better performance in the LFC problem [36] in order to improve STATCOM's ability to keep the frequency within acceptable ranges. The Artificial Rabbits Optimization (ARO) method, which is a novel bio-inspired meta-heuristic approach, is used to fine-tune the suggested PD-PIDA parameters. This algorithm has demonstrated better performance when it comes to the handling of complex real-world situations [37], [38], [39], [40]. The following are some of the most important contributions that this study presents:

- The management of the reactive power that is injected into power systems with the use of a fine-tuned PD-PIDA-controlled STATCOM for boosting the frequency performance of power systems.
- Using a novel meta-heuristic optimization named ARO to fine-tune the PD-PIDA controller's settings.
- Examining how well the suggested ARO-based PD-PIDA-controlled STATCOM performs on two popular IEEE systems, namely the Kundur system and the IEEE 39 bus system.
- The resilience of the suggested PD-PIDA controller will be validated by integrating wind generation into some of the case studies.
- The impact of extending the allowed output ranges of the PD-PIDA regulator above $\pm 5\%$ on the system's frequency performance is being studied.

The following outline constitutes the paper's structure: Section I provides an introduction to the subject of the research. In Section II, one can get a presentation of the mathematical formulas relating to frequency and reactive power. In Section III, both the investigated case study and the STATCOM model are dissected and discussed. In addition to that, the problem formulation and the PD-PIDA regulator configuration have been presented and discussed in Section IV. Furthermore, the ARO optimization technique is described in Section V. In addition, the outcomes of time domain simulations are reviewed in Section VI for a variety of distinct scenarios. Last but not least, the article is being concluded with Section VII.

II. MATHEMATICAL FORMULAS RELATING FREQUENCY AND REACTIVE POWER

In this part, the mathematical formulas relating frequency and reactive power will be discussed in order to illustrate the significance of controlling the frequency performance of a power system through the utilization of VAR regulation. Assume that a synchronous machine is linked, in the manner depicted in Figure. 2, to an infinite bus by use of a transformer and a dual transmission line [41]. Equations (1) and (2), as shown at the bottom of the next page, yield the real and imaginary powers (P and Q) transmitted from the synchronous machine to the infinite bus:

where V_∞ represents the voltage of the infinite busbar in p.u, E_{ex} depicts the excitation voltage in p.u, δ represents

the power angle, X_{tl} represents the equivalent reactance of transmission lines in p.u, X'_{da} depicts the transient reactance in the direct-axis direction in p.u, and X_{tr} depicts the transformer reactance in p.u. Based on the aforementioned relations, the following relationships can be deduced:

$$\frac{\partial P}{\partial \delta} = \frac{V_\infty \cdot E_{ex} \cdot \cos(\delta)}{X_{tl} + X'_{da} + X_{tr}} = \frac{\partial P}{\partial t} \cdot \frac{\partial t}{\partial \delta} = \frac{\partial P}{\partial t} \cdot \frac{1}{\omega}$$
$$= \frac{Q \cdot \left(X_{tl} + X'_{da} + X_{tr}\right)^2 - E_{ex}^2 \cdot X_{tl} + V^2 \cdot X'_{da}}{\left(X_{tl} + X'_{da} + X_{tr}\right) \cdot \left(X'_{da} - X_{tl}\right)} \quad (3)$$

$$\frac{\partial Q}{\partial \delta} = \frac{V_\infty \cdot E_{ex} \cdot \left(X_{tl} - X'_{da} - X_{tr}\right) \cdot \sin(\delta)}{\left(X_{tl} + X'_{da} + X_{tr}\right)^2}$$
$$= \frac{\partial Q}{\omega \partial t} = \frac{\left(X_{tl} - X_{tr} - X'_{da}\right) \cdot P}{\left(X_{tl} + X'_{da} + X_{tr}\right)} \quad (4)$$

where ω signifies the speed of the rotor for the synchronous machine in p.u. By reorganizing the two previous equations, the following two equations can be driven:

$$\frac{\partial P}{\partial t} = \left[\frac{\left(X_{tl} + X'_{da} + X_{tr}\right)}{\left(X'_{da} - X_{tl}\right)} Q + \frac{V^2 \cdot X'_{da} - E_{ex}^2 \cdot X_{tl}}{\left(X'_{da} - X_{tl}\right) \cdot \left(X_{tl} + X'_{da} + X_{tr}\right)}\right] \omega \quad (5)$$

$$\frac{\partial Q}{\partial t} = \frac{\left(X_{tl} - X_{tr} - X'_{da}\right)}{\left(X_{tl} + X'_{da} + X_{tr}\right)} \cdot P \cdot \omega \quad (6)$$

The swing equation can be presented by Equation (7) and the equation of power angle dynamics can be introduced by Equation (8).

$$M \frac{\partial \omega}{\partial t} = P_{mech} - P_{elect} = P_{mech} - P \quad (7)$$

$$\frac{\partial \delta}{\partial t} = \omega - 1 \quad (8)$$

where M represents the synchronous machine angular momentum. Using the state space version of Equations (5)-(8), we may represent the power system as follows:

$$\begin{bmatrix} \&\partial P/\partial t \\ \&\partial Q/\partial t \\ \&\partial \omega/\partial t \\ \&\partial \delta/\partial t \end{bmatrix} = \begin{bmatrix} 0 & \frac{\left(X_{tl}+X'_{da}+X_{tr}\right)}{\left(X'_{da}-X_{tl}\right)}\omega \\ \frac{\left(X_{tl}-X_{tr}-X'_{da}\right)}{\left(X_{tl}+X'_{da}+X_{tr}\right)}\omega & 0 \\ \frac{-1}{M} & 0 \\ 0 & 0 \end{bmatrix} \begin{bmatrix} \frac{V^2 \cdot X'_{da} - E_{ex}^2 \cdot X_{tl}}{\left(X'_{da}-X_{tl}\right)\cdot\left(X_{tl}+X'_{da}+X_{tr}\right)} & 0 \\ 0 & 0 \\ 0 & 0 \\ 1 & 0 \end{bmatrix} \begin{bmatrix} P \\ Q \\ \omega \\ \delta \end{bmatrix}$$
$$+ \begin{bmatrix} 0 \\ 0 \\ \frac{P_{mech}}{M} \\ -1 \end{bmatrix} \quad (9)$$

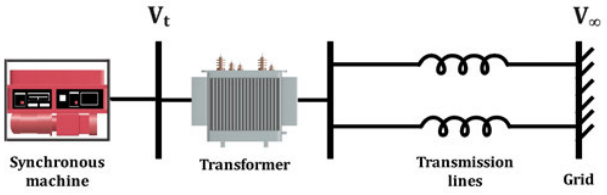

FIGURE 2. The linking of a synchronous machine to an infinite busbar.

As presented in Equation (9), the power system frequency, denoted by ω, is dependent on both real and imaginary power. This implies that increasing the amount of imaginary power that is injected into the system will result in changes to the frequency performance of the system. In addition, the real power of the load, denoted by P_L, is normally proportional to the voltage and may be introduced by a polynomial function in the manner shown below [27]:

$$P_L = P_i \left[b_0 + b_1 \left(\frac{V}{V_i}\right) b_2 \left(\frac{V}{V_i}\right)^2\right] \quad (10)$$

where P_i denotes the initial power of the load in p.u, V_i depicts the initial voltage of the load in p.u, b_0, b_1 and b_2 are the power fractions such that $b_0 + b_1 + b_2 = 1$. From the previous equation, the change in load power may be introduced as follows:

$$\Delta P_L = \frac{\partial P_L}{\partial P_i} \Delta P_i + \frac{\partial P_L}{\partial V} \Delta V \quad (11)$$

The following relation may be obtained by taking the derivative of Equation (10) and then substituting it into Equation (11), where the initial condition $V = V_i = 1$ p.u is used:

$$\Delta P_L = \Delta P_i + \left[(2b_2 + b_1) P_i\right] \Delta V \quad (12)$$

Any variation in V can create a variation in ΔP_L, which in turn influences the frequency of the system, as can be seen from Equation (12), which demonstrates this relationship. The result of inserting capacitive (or leading) imaginary power into the grid is to increase the bus voltages, hence raising the load's real power. In contrast, increasing the amount of inductive (or lagging) imaginary power that is added to the grid would result in lower bus voltages and, as a result, a lower need for real power. In the next section, we are going to talk about the examined system case studies.

$$P = \frac{V_\infty \cdot E_{ex} \cdot \sin(\delta)}{X_{tl} + X'_{da} + X_{tr}} \quad (1)$$

$$Q = \frac{V_\infty \cdot E_{ex} \cdot \left(X_{tr} + X'_{da} - X_{tl}\right) \cdot \cos(\delta) + V_\infty^2 \cdot \left(X'_{da} + X_{tr}\right) + E_{ex}^2 \cdot X_{tl}}{\left(X_{tl} + X'_{da} + X_{tr}\right)^2} \quad (2)$$

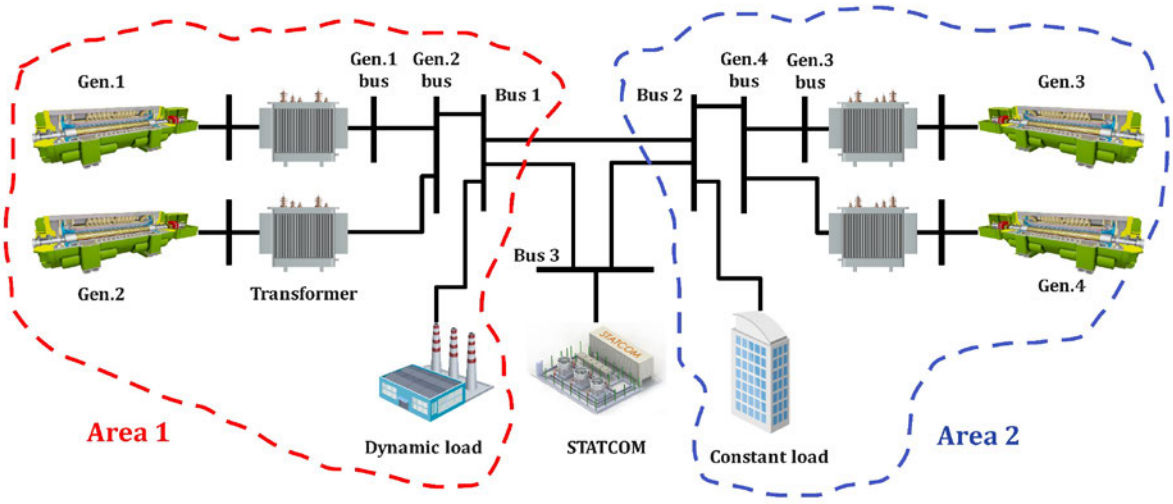

FIGURE 3. The description of the first case study (i.e., Kundur system).

III. THE INVESTIGATED SYSTEM CASE STUDY

On two well-known multi-machine test systems developed and maintained by the IEEE (i.e., the Kundur system and the New England IEEE 39 bus system), the effectiveness of the recommended ARO-based PD-PIDA-controlled STATCOM has been evaluated and modelled.

A. THE DESCRIPTION OF THE KUNDUR SYSTEM

The Kundur system was selected due to the fact that it is widely available in the field of power system research. As can be seen in Figure. 3, it is a dual-area system that has a total of four machines that are linked together by two tie lines, where the governor of each generator is responsible for controlling it. This research made minor adjustments to the model data and setup that were utilized in [27], but otherwise, the two were identical. In order to compare with [35], a 600 MVAR STATCOM unit has been linked to the system through bus 3. Moreover, a simulated load change perturbation is created by applying a controlled dynamic load on bus 1 that has the identical rating as the 967 MW/87 MVAR load, whereas the load in region 2 is simulated by a constant load. Loads, regardless of whether dynamic or static, is proportional to V^2. The prementioned assumptions are taken into consideration in order to provide us with the ability to evaluate how impactful the suggested ARO-based PD-PIDA controlled STATCOM is at controlling the grid frequency in comparison to the STATCOM controlled by MPA-based PIDA regulator described in the earlier research [35].

B. THE DESCRIPTION OF THE IEEE 39 BUS SYSTEM

Athay et al. [42] provided the New England (IEEE 39 bus) system, a huge multi-machine system with 10 generators and 39 buses, and it is depicted in Figure 4. A vast number of generators have been assembled to form Gen. 1. Each machine has an independent governor, and the full set of system settings and starting conditions may be found in [42]. In order to compare with [35] and prove the superiority of the suggested ARO-based PD-PIDA controlled STATCOM at controlling the grid frequency in comparison to the STATCOM controlled by MPA-based PIDA regulator, a 600 MVAR STATCOM unit has been linked to the system through bus 7. Additionally, in order to evaluate the effect that load change has on the frequency response, the greatest load, which is located at bus 8 and has a rating of 576 MW/176 MVAR, is replaced by a controlled dynamic load with an identical power. The static loads are represented by constant impedances. Furthermore, the STATCOM model that was utilised in both of the aforementioned case studies will be discussed in the next part.

C. THE STATCOM MODEL

The STATCOM is a FACTS Voltage Source Converter (VSC) based on a controller which regulates the voltage at its terminal by regulating the imaginary power pumped into the power system. As seen in Figure 6 [43], the control system of the STATCOM unit comprises outside and interior controlling loops. The phase-locked loop (PLL) synchronizes on the three-phase primary voltage V_1's positive sequence component. The three-phase voltage and currents' direct and quadrature-axes components (V_d, V_q, I_d, I_q) are calculated using the PLL's output. The inner current controller receives its reference currents I_{d_Ref} and I_{q_Ref} from an alternating current (AC) voltage regulator and a direct current (DC) voltage regulator in the outside loop. While the PWM converter generates a voltage (V_{2d} and V_{2q}), the magnitude and phase of which are regulated by a current regulator in the interior current regulation loop. Furthermore, a feed-forward type controller helps the current regulator by making predictions about the output voltage V_2 (i.e., V_{2d} and V_{2q}) based on the V_1 value (i.e., V_{1d} and V_{1q}) and the leakage reactance

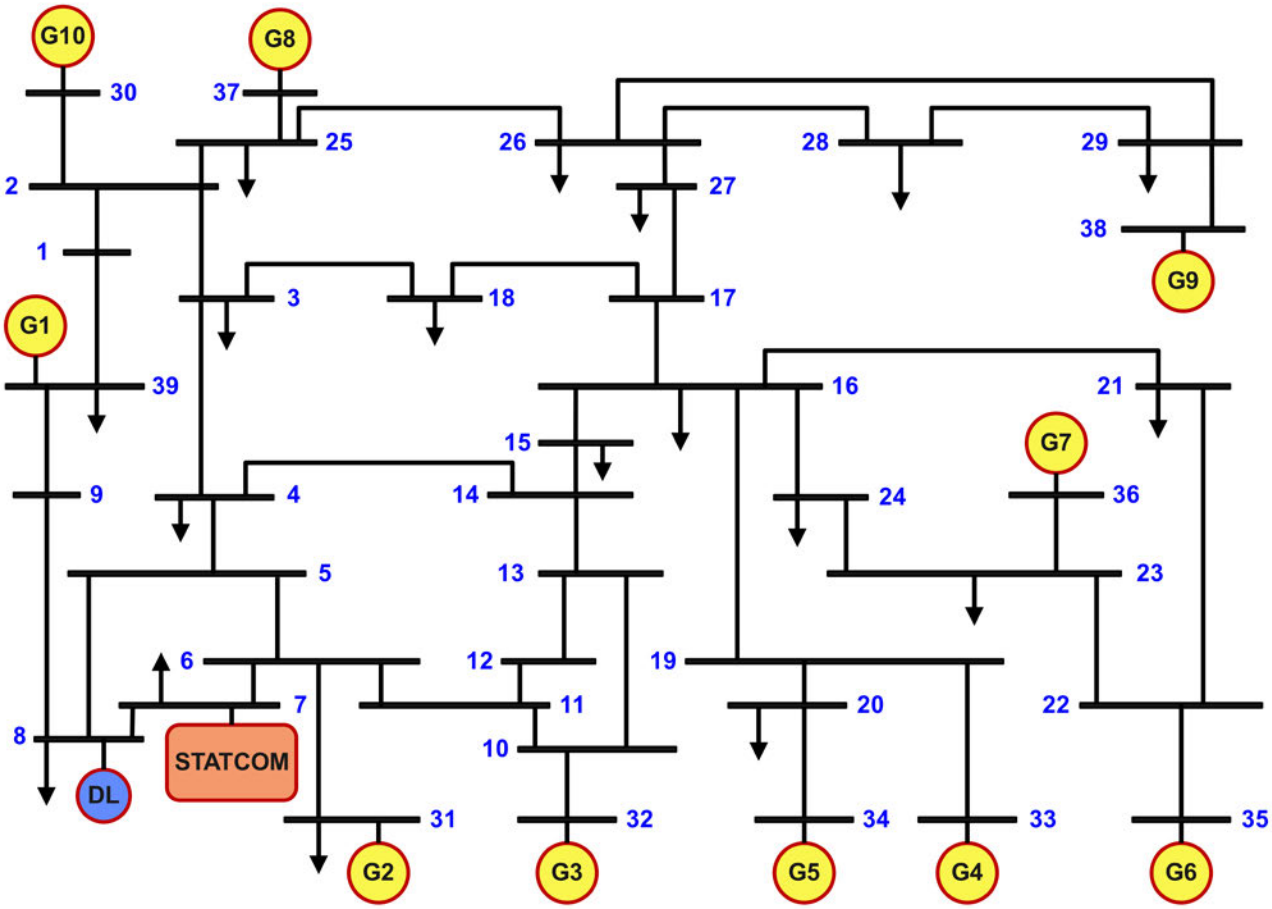

FIGURE 4. The description of the second case study (i.e., New England's ten-machine IEEE 39 bus system).

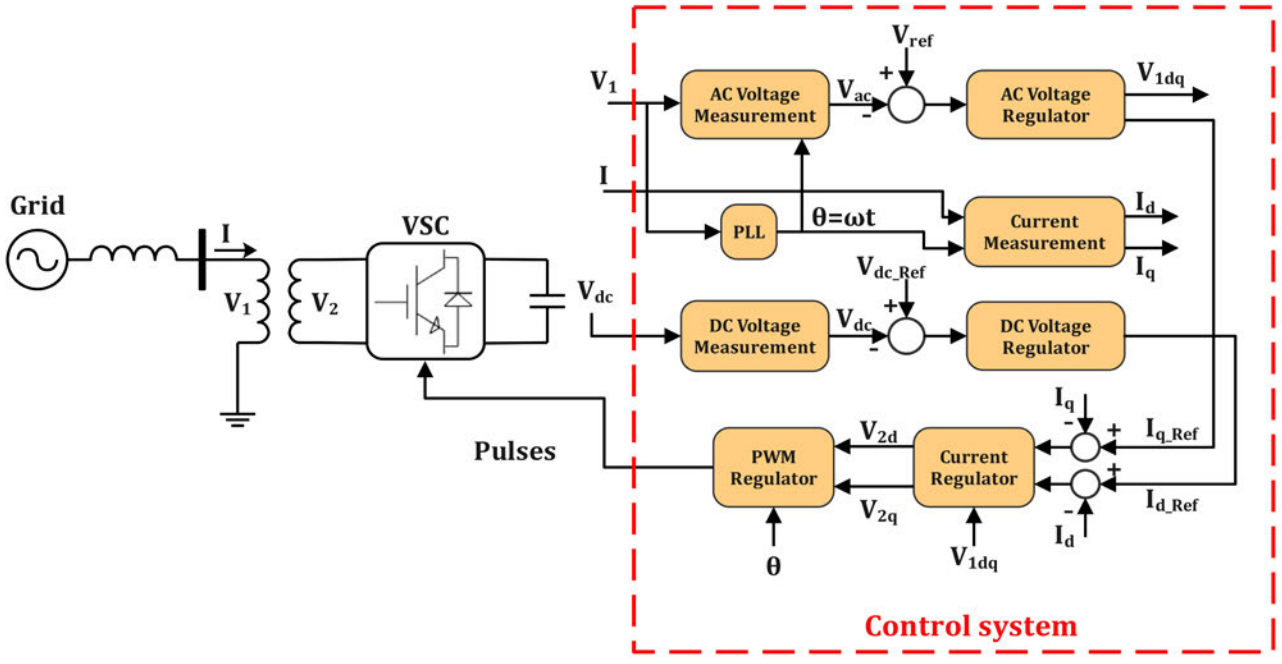

FIGURE 5. The diagram representation of STATCOM [43].

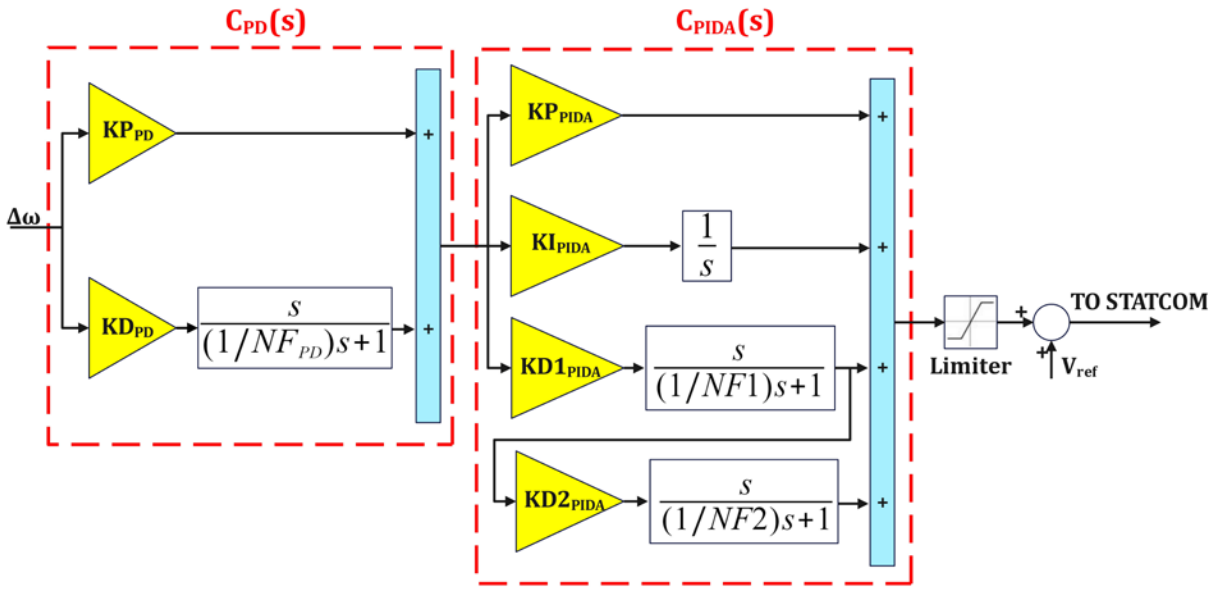

FIGURE 6. The configuration of the suggested PD-PIDA controller.

of the transformer. The next part details the structure of the suggested PD-PIDA regulator and how the problem can be formulated.

IV. PROBLEM FORMULATION AND THE PROPOSED CONTROLLER STRATEGY

The purpose of the control strategy is to boost the performance of frequency for the linked generators of the kundur system. The PD-PIDA regulator that has been developed has nine parameters that have to be their values optimized, and the transfer function of this regulator may be described as follows [36]:

$$C(s) = C_{PD}(s) \cdot C_{PIDA}(s) \tag{13}$$

$$C_{PD}(s) = KP_{PD} + KD_{PD}\left(\frac{s}{\frac{1}{NF_{PD}} \cdot s + 1}\right) \tag{14}$$

$$C_{PIDA}(s) = KP_{PIDA} + \frac{KI_{PIDA}}{s} + KD1_{PIDA}\left(\frac{s}{\frac{1}{NF1} \cdot s + 1}\right) + KD1_{PIDA}KD2_{PIDA} \times \left(\frac{s^2}{\left(\frac{1}{NF1} \cdot s + 1\right) \cdot \left(\frac{1}{NF2} \cdot s + 1\right)}\right) \tag{15}$$

where KP_{PD} and KD_{PD} are the proportional and derivative gains of $C_{PD}(s)$, respectively, and NF_{PD} is the filter coefficient, and KP_{PIDA}, KI_{PIDA}, $KD1_{PIDA}$ and $KD2_{PIDA}$ are the proportional, integral, first-derivative, and second-derivative gains of $C_{PIDA}(s)$, respectively, and $NF1$ and $NF2$ are the filters' coefficients.

The key benefit of the PD-PIDA controller is the enhancement of the system's transient performance by incorporating a double derivative (acceleration) action into the controller structure in addition to the derivative action of the PD controller. A detailed description of the suggested PD-PIDA regulator can be seen in Figure 6. In this structure, the frequency deviation signal ($\Delta\omega$) is sent into the controller, and the controller's output signal is then added to the outside voltage reference (V_{ref}) that is then provided in the STATCOM. A restriction of $\pm 5\% V_{ref}$ is set as the controller's output threshold. Lowering the following objective function ($ObjFn$) yields the optimum settings for the PD-PIDA controller:

$$ObjFn = Min \int_0^{T_{sim}} \left(|\Delta\omega_1|^2 + |\Delta\omega_2|^2 + |\Delta\omega_3|^2 + |\Delta\omega_4|^2\right) dt \tag{16}$$

where T_{sim} represents the simulation time. Additionally, the ARO-based PD-PIDA controller is exposed to the limitations as shown below:

$$\begin{cases} (KP_{PD})_{min} \le KP_{PD} \le (KP_{PD})_{max} \\ (KD_{PD})_{min} \le KD_{PD} \le (KD_{PD})_{max} \\ (NF_{PD})_{min} \le NF_{PD} \le (NF_{PD})_{max} \\ (KP_{PIDA})_{min} \le KP_{PIDA} \le (KP_{PIDA})_{max} \\ (KI_{PIDA})_{min} \le KI_{PIDA} \le (KI_{PIDA})_{max} \\ (KD1_{PIDA})_{min} \le KD1_{PIDA} \le (KD1_{PIDA})_{max} \\ (KD2_{PIDA})_{min} \le KD2_{PIDA} \le (KD2_{PIDA})_{max} \\ (NF1)_{min} \le NF1 \le (NF1)_{max} \\ (NF2)_{min} \le NF2 \le (NF2)_{max} \end{cases} \tag{17}$$

where the lower boundaries are chosen as [0, 0, 100, 0, 0, 0, 0, 100, 100] while the upper boundaries are chosen as [50, 10, 400, 100, 100, 10, 0.05, 400, 400]. The following section describes the ARO optimization approach that was

employed during the development of the suggested PD-PIDA regulator.

V. ARTIFICIAL RABBITS OPTIMIZER (ARO)

A. WHY ARO IS THE CHOSEN ALGORITHM

Only issues that are convex can be solved using traditional optimization strategies. It may turn non-convex problems into convex ones within certain approximations [44]. It is recommended to use metaheuristic approaches rather than approximations when attempting to transform a present non-linear and non-convex issue into a convex problem before attempting to optimize the solution with traditional methods. The Artificial Rabbits Optimizer (ARO) technique is one of the newest metaheuristic techniques in 2022. As mentioned in [37], the ARO algorithm outperforms famous metaheuristic approaches such as Teaching Learning-Based optimizer (TLBO), Particle Swarm Optimizer (PSO), Atom Search Optimizer (ASO), Gravitational Search Algorithm (GSA), Artificial Bee Colony (ABC), Differential Evolution (DE) and Cuckoo Search (CS). ARO satisfies the requirements of the Global Search Convergence theory. According to the theory, ARO simply can't fail to reach the global optimal. As a consequence, the optimization issue in this article is handled successfully by ARO.

B. ARO INSPIRATION AND CONCEPT

The essence of the survival methods used by rabbits acted as the core for the genesis of the algorithm that is used by ARO. When they are being pursued by predators, rabbits will use one of two primary survival tactics: the first tactic is known as detour foraging, and the second one is known as random hiding from adversaries [37].

The detour foraging strategy is dependent on the sorts of food consumed by rabbits, which include grass, weeds, and forbs. Rabbits will not eat the grass that is close to their nest holes since this puts them at risk of being attacked by a predator. Instead, they will continuously search for food that is further away from their nests. Rabbits have an unusually broad field of vision, which allows them to identify food sources across a large region. This visual field is dependent on overhead scanning. The tactic of making a detour in order to forage is an example of exploration. This strategy for survival is so widely known that there is even an adage in Chinese that describes it: ''rabbits do not eat the grass near their own nest.''

The rabbit's second method for ensuring its own survival is to conceal itself in an unpredictable manner. As shown in the picture of Figure 7, rabbits will dig a number of burrows in the area surrounding their nests in order to deceive their enemies and to make the process of escaping their territory simpler. This is especially true if the rabbits randomly select one of the burrows as a place to take refuge from their enemies. Since rabbits have small forelegs and long hind legs, as well as powerful muscles and tendons, they are able to sprint quite quickly. This is made possible by their bodily structure. In addition to this, rabbits have the ability to throw off their

FIGURE 7. The nest has several burrows [45].

pursuers by fleeing in a zigzag pattern, pausing unexpectedly while running and making abrupt turns.

The second tactic is known as the exploitation approach. Because sprinting quickly causes energy shrink, rabbits need to be able to dynamically shift between detour foraging and random hiding according to how much energy they have.

C. MATHEMATICAL DESCRIPTION OF ARO

Only ARO utilizes the foraging and hiding techniques of genuine rabbits, along with their energy shrink first to transit between both methods. The ARO algorithm's mathematical model is split into three key aspects. These are the following: detour foraging or exploration, random hiding or exploitation, and energy shrink limitation. In [37], the mathematical model is dissected down into its constituent components and examined in depth.

The ARO technique, like other meta-heuristics, proposes random answers as the starting point for its computations. Assuming the number of rabbit populations is n, identical to the number of arbitrary solutions that are required. This procedure is seen in Figure 8. The ARO algorithm's starting population is specified as Equation (18).

$$Population = \begin{bmatrix} x_1^1 & \cdots & x_1^{dim} \\ \vdots & \ddots & \vdots \\ x_n^1 & \cdots & x_n^{dim} \end{bmatrix} \tag{18}$$

where n is the population size and dim is the variables' dimension, and considering that the purpose is to fine-tune the parameters of the proposed PD-PIDA (KP_{PD}, KD_{PD}, NF_{PD}, KP_{PIDA}, KI_{PIDA}, $KD1_{PIDA}$, $KD2_{PIDA}$, $NF1$ and $NF2$), thus dim is equal to 9. Equation (19) is used to generate each possible solution at random.

$$\vec{x}_\alpha = LB + [UB - LB] \cdot rand\,(1, dim)\,, \alpha = 1, \ldots, n \tag{19}$$

where $\vec{x}_\alpha$ denotes the location of the rabbit, LB and UB denote the lower and upper bounds of the controller's parameters,

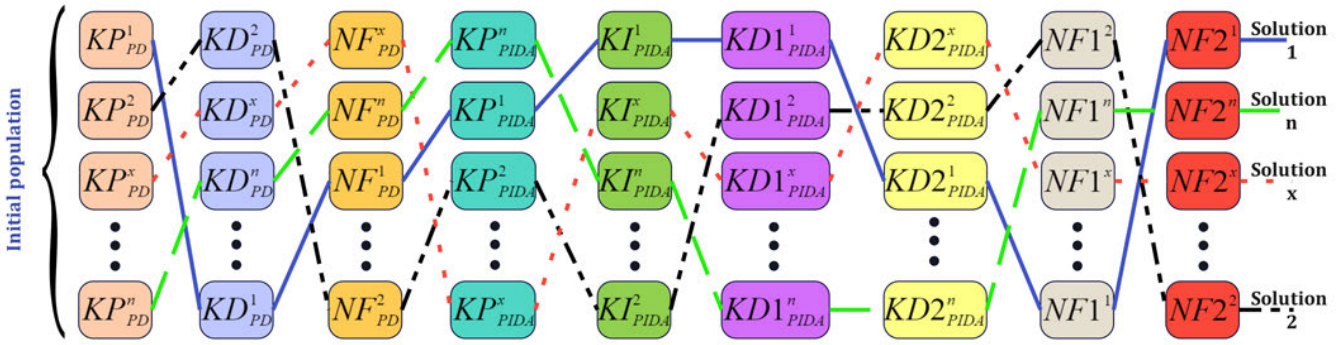

FIGURE 8. The initialization process of the solutions with the ARO approach.

and n and dim denote the population size and number of the controller's parameters, respectively.

1) DETOUR FORAGING (EXPLORATION)

In ARO, let's say that each rabbit in the group has its own region that has some grass and d burrows, and that the rabbits feed by arbitrarily wandering to the position of each other. When they are hungry, rabbits will usually wander about in circles looking for food until they find enough to eat. The ARO detour foraging behavior thus means that each search individual has a tendency to update its location towards the other search individual chosen at random from the group and contributes a disruption to the situation. The mathematical formalism of the rabbits' detour foraging behavior is provided by the following:

$$\begin{aligned}\vec{v}_{\alpha}(t+1) &= \vec{x}_{\beta}(t) + Y \cdot \left(\vec{x}_{\alpha}(t) - \vec{x}_{\beta}(t)\right) \\ &\quad + round\left(0.5 \cdot (0.05 + y_1)\right) \cdot n_1, \alpha, \beta \\ &= 1, \ldots, n \text{ and } \beta \neq \alpha \end{aligned} \tag{20}$$

$$Y = L \cdot u \tag{21}$$

$$L = \left(e - e^{\left(\frac{t-1}{M}\right)^2}\right) \cdot \sin(2\pi y_2) \tag{22}$$

$$\begin{aligned} u(k) &= \begin{cases} 1 & if k == q(l) \\ 0 & else \end{cases} k = 1, \ldots, d \quad and \ l \\ &= 1, \ldots, [y_3 \cdot d] \end{aligned} \tag{23}$$

$$q = randperm(d) \tag{24}$$

$$n_1 \sim N(0, 1) \tag{25}$$

where $\vec{v}_{\alpha}(t+1)$ denotes the α^{th} rabbit's location at time $t+1$, $\vec{x}_{\beta}(t)$ denotes the α^{th} rabbit's position at time t, n depicts the rabbit's population size, d denotes the problem's dimension, M denotes the maximum number of iterations, *round* depicts rounding to the closest integer number, *rand perm* gives a random permutation of the integers within the range 1 to d, y_1, y_2 and y_3 denote three arbitrary values from zero to unity, l represents the running length while performing the detour foraging, and n_1 depicts the subject to the standard normal distribution.

Searching individuals, as shown by Equation (20), conduct their foraging searches at random with respect to one another. By taking this step, a rabbit might move to the territory of the other rabbits, which is located far away from its original territory. In particular, a rabbit's decision to visit the nests of other rabbits rather than its own makes a significant contribution to exploration and ensures the ARO algorithm's capacity to identify global search.

2) RANDOM HIDING (EXPLOITATION)

For each iteration of the ARO approach, a rabbit produces d arbitrary burrows in all directions along the search space. If it wants to lessen its chances of being attacked, it will choose a burrow as its hiding place. For the α^{th} rabbit, the β^{th} burrow is produced by:

$$\begin{aligned}\vec{b}_{\alpha,\beta}(t) &= \vec{x}_{\alpha}(t) + P \cdot q \cdot \vec{x}_{\alpha}(t), \alpha \\ &= 1, \ldots, n \text{ and } \beta = 1, \ldots, d \end{aligned} \tag{26}$$

$$P = \frac{M - t + 1}{M} \cdot y_4 \tag{27}$$

$$n_2 \sim N(0, 1) \tag{28}$$

$$q(k) = \begin{cases} 1 & if \ k == \beta \\ 0 & else \end{cases} k = 1, \ldots, d \tag{29}$$

Based on Equation (26), there will be a total of d burrows in close proximity to a rabbit in all directions. The hiding parameter, P, undergoes a linear reduction from 1 to M^{-1} with an arbitrary fluctuation throughout the iterative process. In accordance with this criterion, rabbits first dig their burrows in a wider area around their home. With more and more iterations, this area will be shrunk. When looking for a safe place to hide, rabbits choose a burrow at random. Using the following equations, we can represent this haphazard method of hiding mathematically as follows:

$$\begin{aligned}\vec{v}_{\alpha}(t+1) = \vec{x}_{\alpha}(t) + Y \cdot \left(y_4 \cdot \vec{b}_{\alpha,y}(t) - \vec{x}_{\alpha}(t)\right), \\ \alpha = 1, \ldots, n \end{aligned} \tag{30}$$

$$q_y(k) = \begin{cases} 1 & if\ k == \lceil y_5 \cdot d \rceil \\ 0 & else \end{cases} k = 1, \ldots, d \quad (31)$$

$$\vec{b}_{\alpha,y}(t) = \vec{x}_\alpha(t) + P \cdot q_y \cdot \vec{x}_\alpha(t) \quad (32)$$

where $\vec{b}_{\alpha,y}(t)$ is an arbitrarily chosen burrow from d burrows for the rabbit to hide, y_4 and y_5 denote two arbitrary values from the range 0 to 1.

The α^{th} Search individual is going to update its location in relation to the randomly chosen burrow among the d burrows using Equation (30). Following the successful completion of either detour foraging or random hiding, the α^{th} rabbit's location is updated as follows:

$$\vec{x}_\alpha(t+1) = \begin{cases} \vec{x}_\alpha(t) f(\vec{x}_\alpha(t)) \leq f(\vec{v}_\alpha(t+1)) \\ \vec{v}_\alpha(t+1) f(\vec{x}_\alpha(t)) > f(\vec{v}_\alpha(t+1)) \end{cases} \quad (33)$$

The preceding formula indicates that the α^{th} the rabbit will leave its current location in favor of a candidate one produced by either Equation (20) or (30), depending on whose fitness is better.

3) ENERGY SHRINK (SHIFT FROM EXPLORATION TO EXPLOITATION)

To depict the shift from exploration to exploitation, an energy factor needs to be determined. The following formula, with y standing in for any arbitrary number between 0 and 1, is used to define the energy factor of ARO:

$$A(t) = 4 \cdot \left(1 - \frac{t}{M}\right) \cdot ln\frac{1}{y} \quad (34)$$

In ARO, when the energy factor $A(t)$ is more than one, a rabbit is sited to arbitrarily find the regions of forage for other rabbits in the exploration phase. Thereafter, the phase of detour foraging takes place; when the energy factor $A(t)$ is less than or equal to one, a rabbit is encouraged to arbitrarily plunder its burrows during the exploitation phase; thus, the phase of random hiding takes place. ARO is capable of switching between the random hiding strategy and the detour foraging strategy based on the value of the energy factor A. As the number of iterations rises, the energy factor A drops, which makes it easier for each individual in the population to shift between the action of detour foraging and random hiding. Once the termination condition has been met, then the most effective solution will be compensated, and all of the updates will have been successfully implemented. Figure 9 shows the flow chart representation of ARO. In the next section, the outcomes of time domain simulations are reviewed.

VI. SIMULATION RESULTS AND DISCUSSION

In this section, two case studies have been discussed. The first case highlighted the frequency performance of the Kundur system when exposed to numerous disturbances that, among other things, will have an effect on the frequency response of all generators. These include:

- **Case A.1:** Impact of 20% loss in the dynamic load.
- **Case A.2:** Impact of multi-step load profile.
- **Case A.3:** Impact of generator 2 (Gen.2) disconnection.
- **Case A.4:** Impact of elevating the restriction from the controller output.
- **Case A.5:** Impact of 20% loss in the dynamic load with wind farm integration in area 2.
- **Case A.6:** Impact of Gen.2 disconnection with wind farm integration in area 2.

The second case study highlighted the frequency performance of the New England 39 bus system when exposed the following disturbances:

- **Case B.1:** Impact of 20% loss in the dynamic load.
- **Case B.2:** Impact of generator 4 (Gen.4) disconnection.

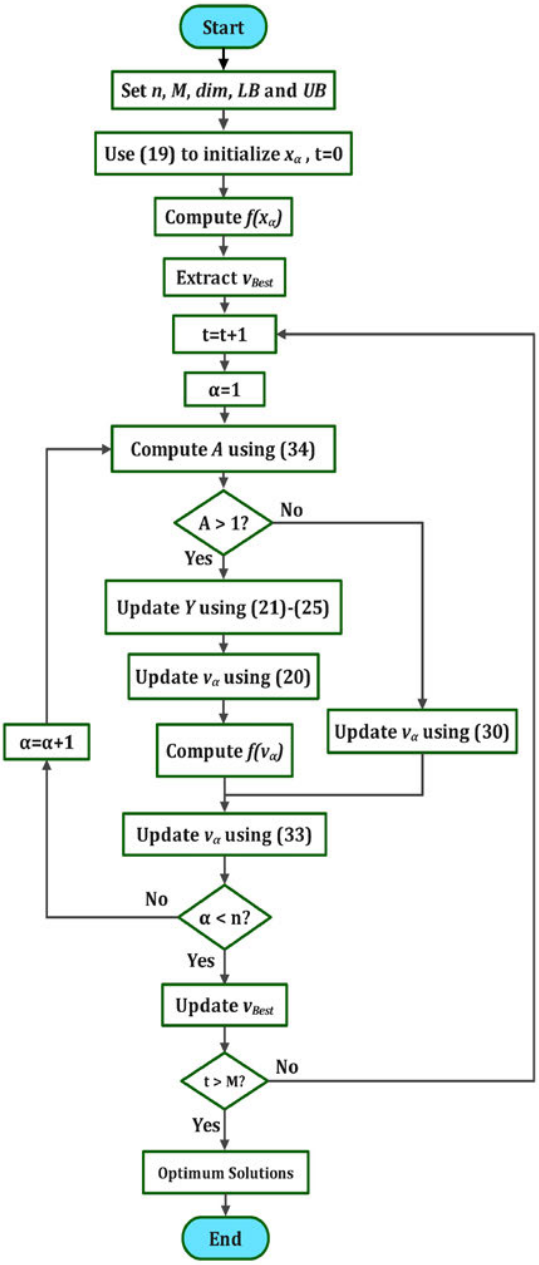

FIGURE 9. The ARO flow chart [37].

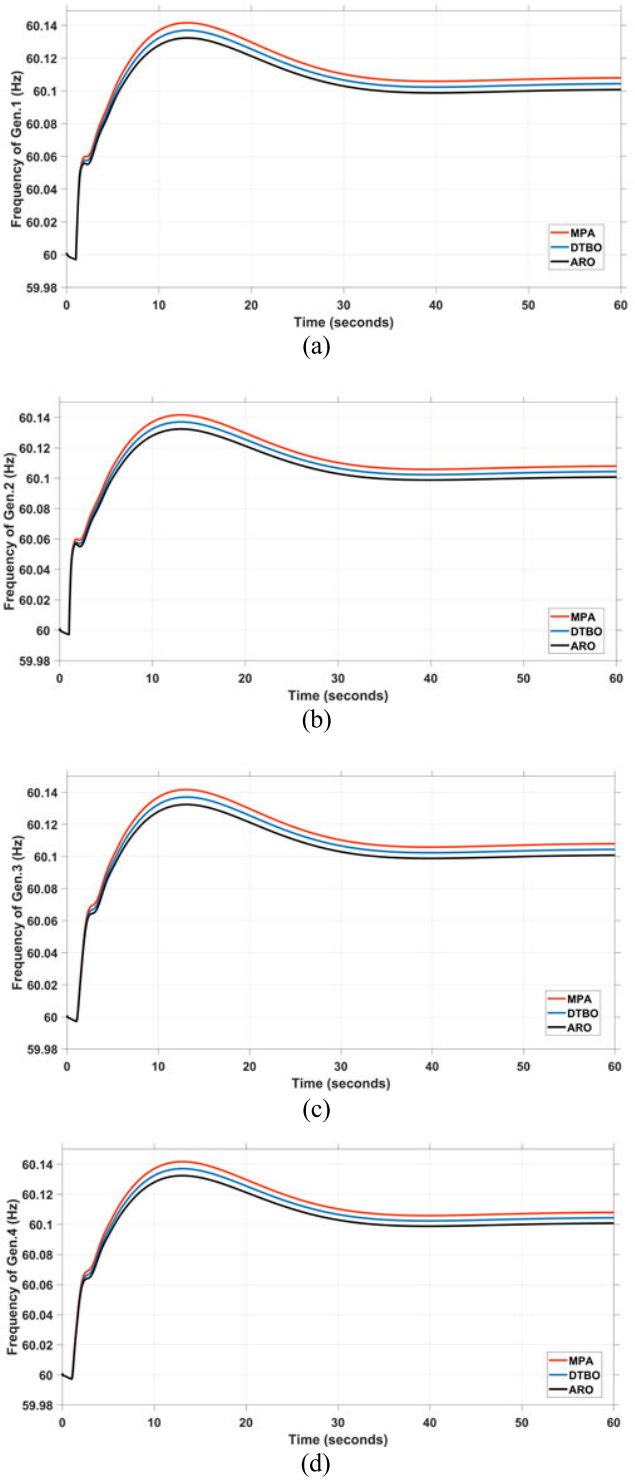

FIGURE 10. The impact of a 20% load loss on the Generators' frequencies using various optimization approaches.

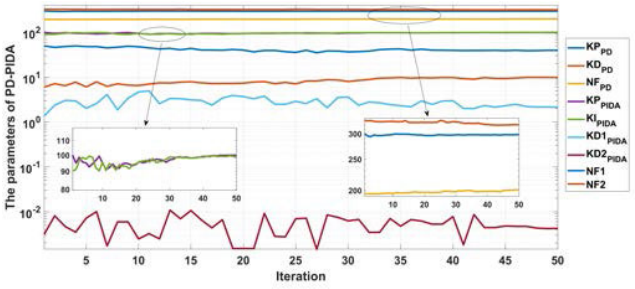

FIGURE 11. The variation of the proposed controller parameters during the optimization process.

TABLE 1. Optimum settings of the comparative controllers with ± 5% output limits.

Controllers	Parameters								
	KP_{PD}	KD_{PD}	NF_{PD}	KP_{PIDA}	KI_{PIDA}	$KD1_{PIDA}$	$KD2_{PIDA}$	$NF1$	$NF2$
MPA based PIDA [35]	N/A	N/A	N/A	30	4.535	6.401	0.0012	280	300
MPA based PD-PIDA	31.45	5.48	325	45.8	32.45	5.421	0.0245	291	312
DTBO based PD-PIDA	35.9	8.78	250.6	85.7	90.54	3.233	0.0015	360	345
ARO-based PD-PIDA (proposed)	39.82	9.87	200.8	100	98.6	2.124	0.0042	298	320

TABLE 2. The impact of a 20% load loss on the system dynamics using various optimization approaches.

Variables	MPA	DTBO	ARO (proposed)
Max. O. (Hz)	60.141	60.134	60.128
St. St. Frequency (Hz)	60.108	60.1044	60.1

TABLE 3. The impact of a 20% load loss on the system dynamics.

	Variables	Without STATCOM	MPA based PIDA STATCOM [33]	ARO-based PD-PIDA STATCOM
Generators	Max. O. (Hz)	60.251	60.164	60.128
	St. St. Frequency (Hz)	60.2	60.124	60.1
STATCOM	St. St. Q (Mvar)	N/A	-130.6	-175.2

A. THE KUNDUR SYSTEM CASE STUDY

1) IMPACT OF 20% LOSS IN THE DYNAMIC LOAD

This section compares the proposed ARO-based PD-PIDA controlled STATCOM to the MPA-based PIDA STATCOM and the NO STATCOM case. Furthermore, demonstrates the efficiency of the suggested algorithm (i.e., ARO [37]) over other metaheuristic optimization strategies such as the Marine Predator Algorithm (MPA) [46] and Driving Training-Based Optimizer (DTBO) [47]. In this case, Area 1 of the examined system is exposed to a 20% load loss. Table 1 provides a summary of the optimum parameters for both the MPA-based

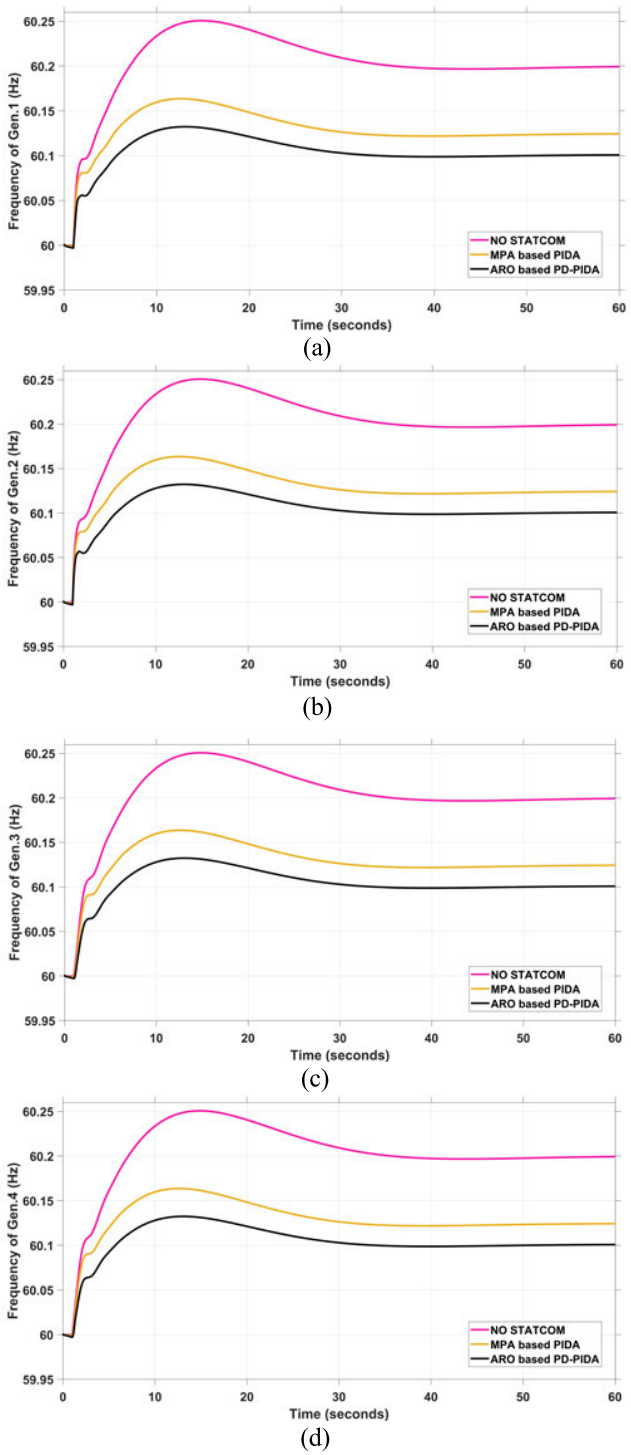

FIGURE 12. The impact of a 20% load loss on the Generators' frequencies (a) Gen.1, (b) Gen.2, (c) Gen.3, and (d) Gen.4.

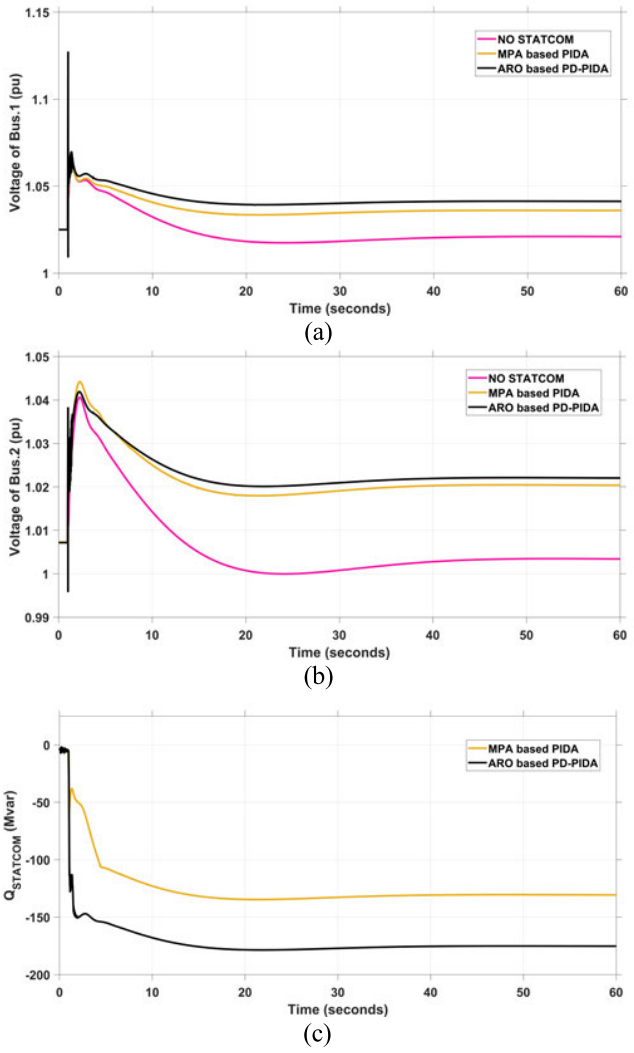

FIGURE 13. The impact of a 20% load loss on (a) Vbus.1, (b) Vbus.2, and (c) QSTATCOM.

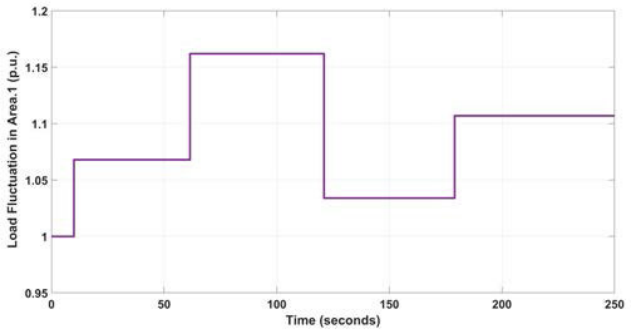

FIGURE 14. Multi-step load profile.

PIDA STATCOM and the PD-PIDA controlled STATCOM that is tuned by MPA, DTBO, and ARO. The ARO algorithm has a superior frequency response compared to other algorithms, as seen in Figure 10. Despite the fact that the 5% limiter effect makes the distinction between the analyzed optimization strategies relatively insignificant, the ARO nevertheless delivers a superior frequency response with less overshoot (Max. O.) and better steady-state frequency (St. St. Frequency) than the other techniques. The dynamics of the system are outlined in Table 2. Figure 11 also shows how the parameters of the proposed PD-PIDA controller changed as the ARO algorithm worked to improve them.

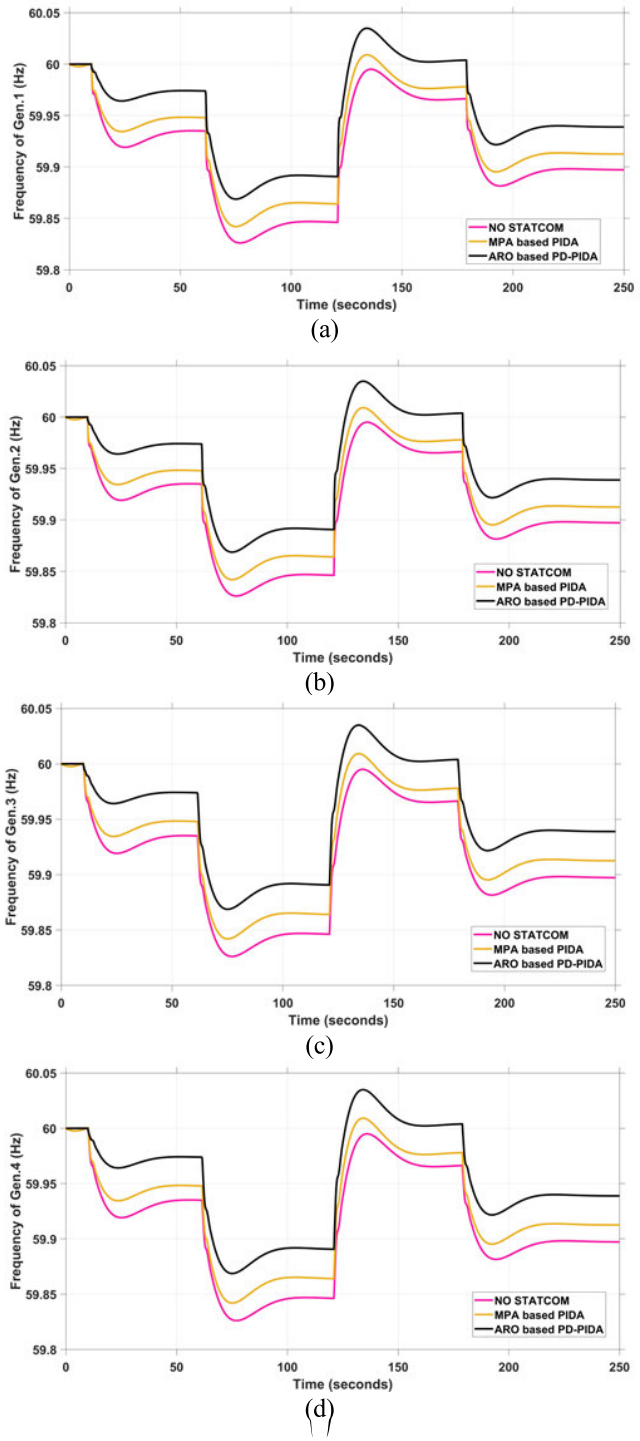

FIGURE 15. The impact of a multi-step load fluctuation in area 1 on the Generators' frequencies (a) Gen.1, (b) Gen.2, (c) Gen.3, and (d) Gen.4.

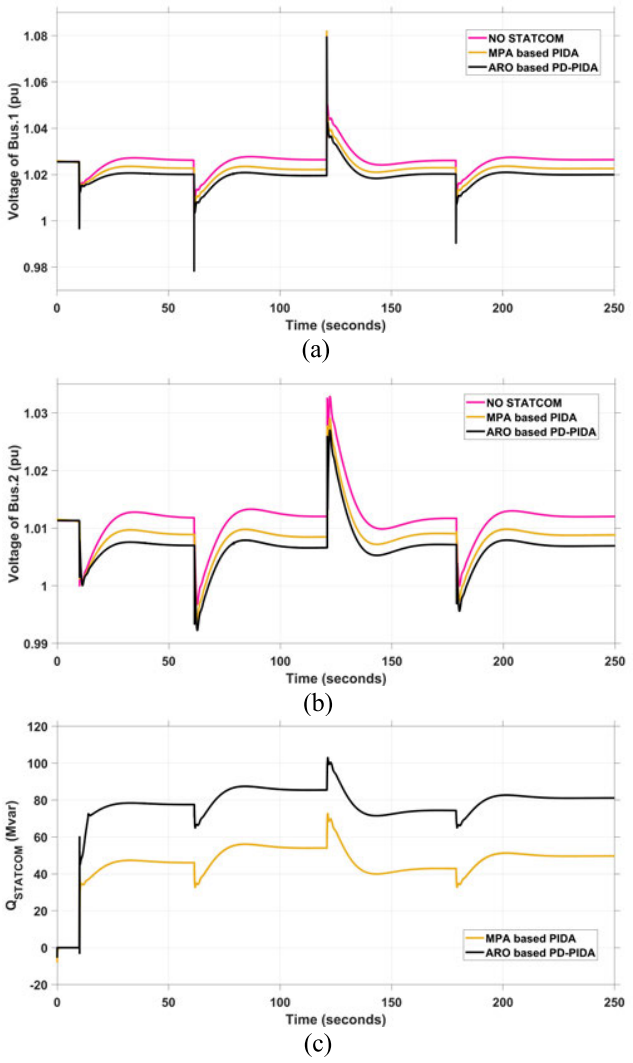

FIGURE 16. The impact of a multi-step load fluctuation in area 1 on (a) Vbus.1, (b) Vbus.2, and (c) QSTATCOM.

Figure. 12 shows that If STATCOM is not applied, the grid frequency will rise to 60.251 Hz as soon as the regarded disturbance takes place. When the MPA-based PIDA-controlled STATCOM is implemented, this Max. O. is brought down to a frequency of 60.164 Hz. In addition to this, when the ARO-based PD-PIDA controller is utilized, the frequency overshoots to just 60.128 Hz. Additionally, the suggested regulator was successful in attaining the lowest St. St. value of the frequency (60.1 Hz). In addition to this, as can be shown in Figure 13 (c), the ARO-based PD-PIDA-driven STATCOM offers a greater amount of transient capacitive power than the MPA-based PIDA. This results in an increase in the load bus voltage, as can be shown in Figure 13 (a) and (b), and therefore leads to an increase in the connected demand as a means of attempting to compensate for the lower load. Table 3 lists the system dynamics of this issue.

2) IMPACT OF MULTI-STEP LOAD PROFILE

This scenario is employed to assess the proposed ARO-based PD-PIDA controlled STATCOM's ability to withstand a change in load in area 1, as seen in Figure 14. To keep the effective load change to a minimum when the load climbs over its original value at 10 s, the STATCOM unit will often have a tendency to reduce the load bus voltages by taking

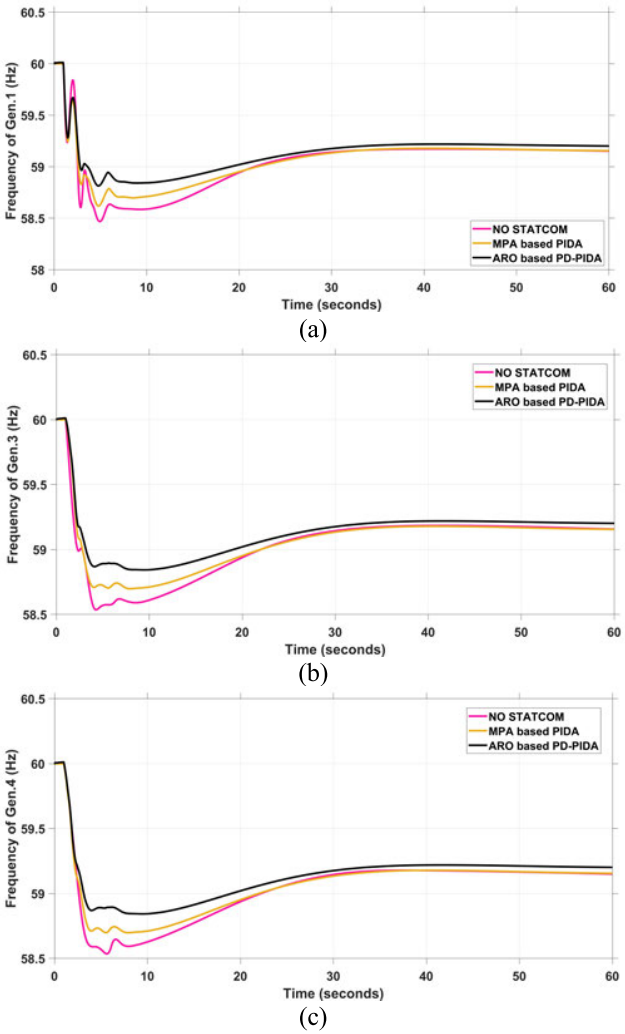

FIGURE 17. The impact of Gen.2 disconnection on the Generators' frequencies (a) Gen.1, (b) Gen.3, and (c) Gen.4.

additional imaginary power (inductive form). This will occur when the STATCOM detects that the load has increased above its starting value (as the demand is proportional to V^2). Furthermore, as shown in Figures 15 and 16, the STATCOM controlled by ARO-based PD-PIDA regulator drains more imaginary power than the MPA-based PIDA. This results in a reduction in the bus voltages as well as the effective load change, which in turn leads to a superior frequency performance that has a low steady-state error regardless of the load fluctuation.

3) IMPACT OF GEN.2 DISCONNECTION

When Gen.2 is removed, the frequency performance of the other linked generators drops to 58.5 Hz in the NO STATCOM case. When employing the suggested ARO-based PD-PIDA controlled STATCOM, the frequency response is improved to 58.89 Hz, which results in reduced undershoot (Max. U.) and better St. St. frequency in comparison to the MPA-based PIDA scenario, which has a Max. U. of 58.7 Hz. All of these characteristics can be seen in

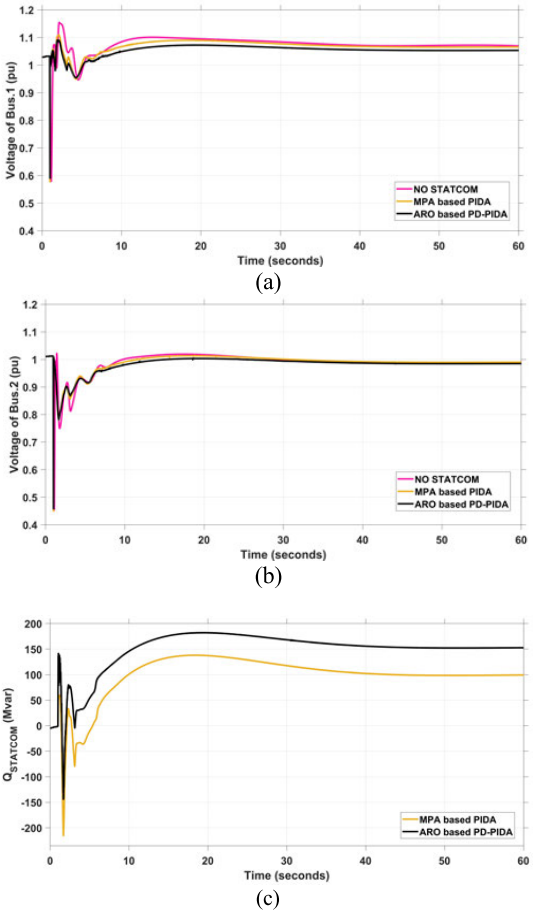

FIGURE 18. The impact of Gen.2 disconnection on (a) Vbus.1, (b) Vbus.2, and (c) QSTATCOM.

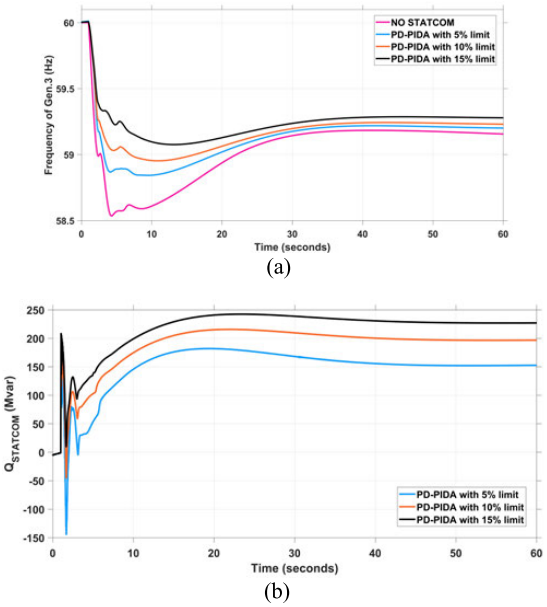

FIGURE 19. The impact of elevating the restrictions from the controller output on (a) Frequency of Gen.3 and (b) QSTATCOM.

Figure 17. By supplying more transient inductive power, as shown in Figure 17 (c), the ARO-based PD-PIDA-

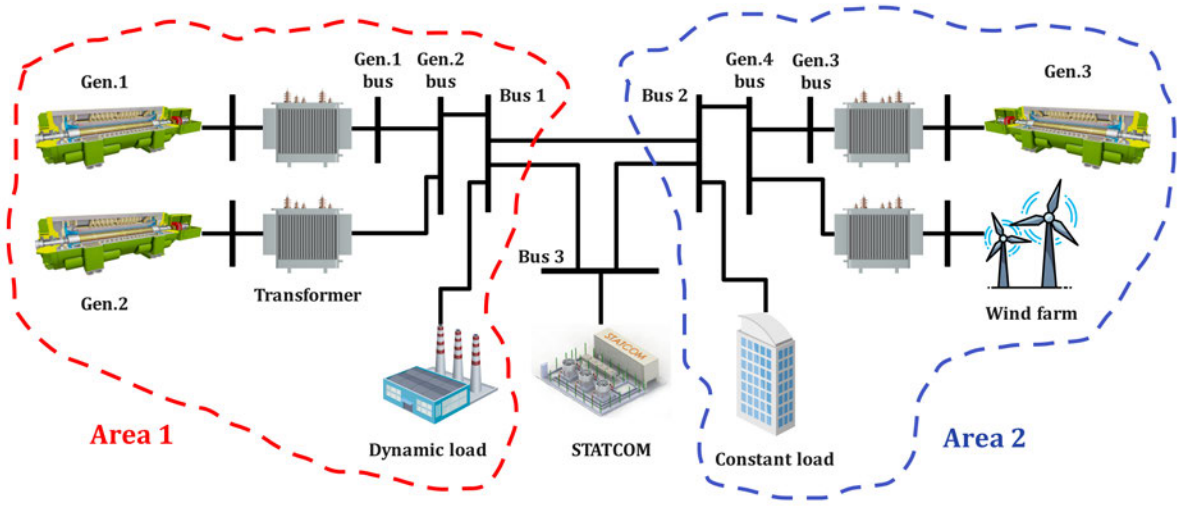

FIGURE 20. The investigated Kundur system description with wind integration.

TABLE 4. The impact of Gen.2 disconnection on system dynamics.

Generators	Variables	Without STATCOM	MPA based PIDA STATCOM [35]	ARO-based PD-PIDA STATCOM
Gen.1	Max. U. (Hz)	58.472	58.628	58.86
	St. St. Frequency (Hz)	59.151	59.155	59.25
Gen.3	Max. U. (Hz)	58.538	58.71	58.89
	St. St. Frequency (Hz)	59.155	59.156	59.32
Gen.4	Max. U. (Hz)	58.5	58.698	58.89
	St. St. Frequency (Hz)	59.15	59.155	59.25
STATCOM	St. St. Q (Mvar)	N/A	100	152.7

controlled STATCOM helps to preserve the generation load balance, as described in Figures 18 (a) and (b). This is accomplished by slightly lowering the voltages of load buses and, in turn, the attached load demand. Table 4 provides a concise summary of the system dynamics relevant to this case study.

4) IMPACT OF ELEVATING THE RESTRICTION FROM THE CONTROLLER OUTPUT

Within this part, the impact of elevating the permitted output restrictions of the PD-PIDA regulator above ±5% on the frequency performance of the Kundur system is dissected and discussed. Within the scope of this investigation, the output of the ARO-based PD-PIDA regulator is given the opportunity to be restricted twice, at ±10% and ±15%, respectively. When the system is subjected to Gen.2 disconnection, for every ±5% increase in the STATCOM output limits, the St. St. frequency is enhanced by 0.04 Hz, and the Max. U. frequency is more lowered by 0.07 Hz, as shown in Figure 19 (a). Additionally, as shown in Figure 19 (b), the amount of reactive power delivered by the STATCOM increases proportionally with the permitted voltage limitations. The performance

TABLE 5. The impact of elevating the restrictions from the controller output on the system dynamics.

Generators	Variables	Without STATCOM	PD-PIDA STATCOM limits ±0.05 pu	±0.1 pu	±0.15 pu
Gen.3	Max. U. (Hz)	58.538	58.89	58.96	59.1
	St. St. Frequency (Hz)	59.155	59.32	59.34	59.37
STATCOM	St. St. Q (Mvar)	N/A	152.7	196.9	227.1

TABLE 6. The impact of a 20% load loss on system dynamics with wind farm integration.

	Variables	Without STATCOM	MPA based PIDA STATCOM [35]	ARO based PD-PIDA STATCOM
Generators	Max. O. (Hz)	60.294	60.241	60.198
	St. St. Frequency (Hz)	60.241	60.181	60.127
STATCOM	St. St. Q (Mvar)	N/A	-79.19	-135.43

of the system with configurable STATCOM restrictions is listed in Table 5. This approach has the potential to increase the frequency response within certain limitations and may be utilized as an extra way for controlling frequency. If regulations make it possible for the voltage of the system to fluctuate by more than 5% in the event of an emergency, regulated reactive power sources that are linked to the grid will be able to provide additional advantages in terms of the primary frequency response.

5) IMPACT OF 20% LOSS IN THE DYNAMIC LOAD WITH WIND FARM INTEGRATION IN AREA 2

The purpose of this subsection is to test the robustness of the presented STATCOM controlled by the ARO-based

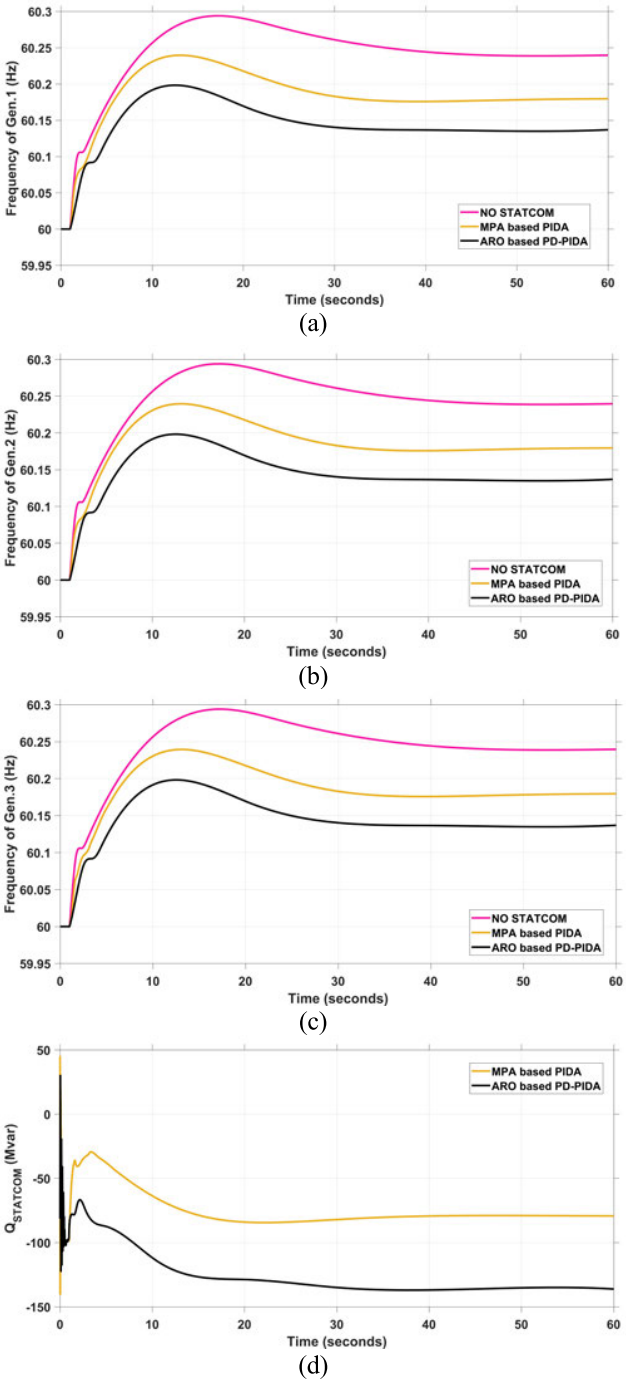

FIGURE 21. The impact of a 20% load loss on system dynamics with wind farm integration (a) Frequency of Gen.1, (b) Frequency of Gen.2, (c) Frequency of Gen.3, and (d) QSTATCOM.

PD-PIDA when a wind farm is incorporated into the examined system. Within this particular scenario, as indicated in Figure 20, we used the assumption that Gen.4 in area 2 is changed out for a DFIG wind farm system with an identical power rating. In Figure 21 The suggested PD-PIDA controller improves the Max. O. frequency of the Kundur system to 60.198 Hz and the St. St. frequency to 60.127 Hz when exposed to an abrupt 20% load loss. Furthermore,

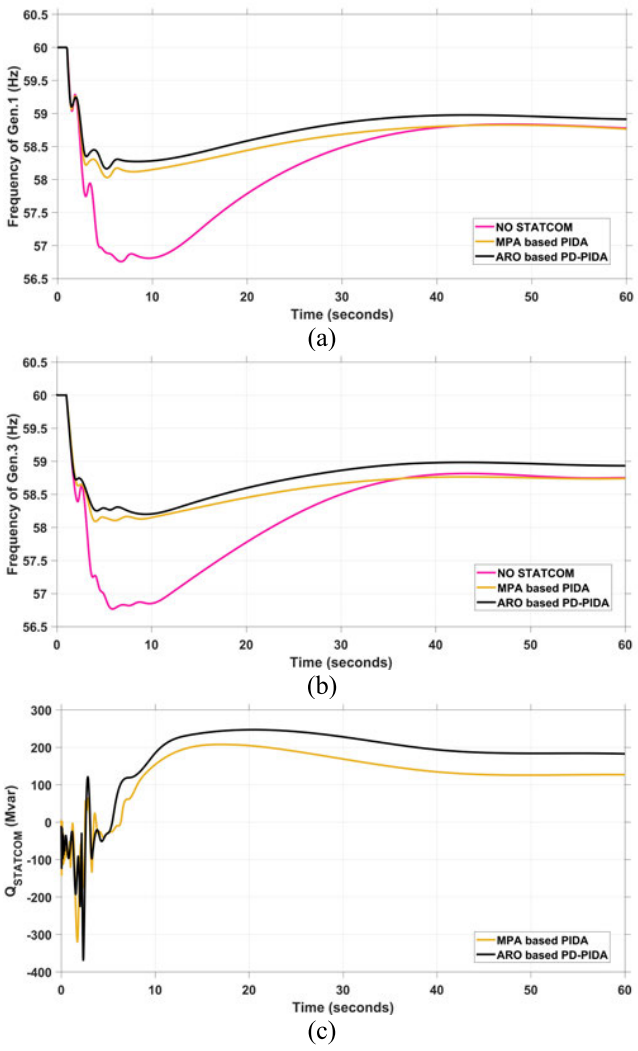

FIGURE 22. The impact of Gen.2 disconnection on system dynamics with wind farm integration (a) Frequency of Gen.1, (b) Frequency of Gen.3, (c) QSTATCOM.

the STATCOM controlled by ARO-based PD-PIDA delivers more transient capacitive power (135.43 Mvar) than the one controlled by the MPA-based PIDA. This is despite the fact that the system shows somewhat larger overshoots caused by reduced inertia due to the existence of the wind farm system. Table 6 provides a concise summary of the system performance characteristics related to this scenario.

6) IMPACT OF GEN.2 DISCONNECTION WITH WIND FARM INTEGRATION IN AREA 2

Herein, not only the wind farm integration in area 2 will take effect, but also Gen.2 will be disconnected. According to the analysis, the ARO-based PD-PIDA regulator offers a superior frequency performance when put in a comparison with the other strategies. The Max. U. frequency is capped at 58.26 Hz with the help of the suggested PD-PIDA controller and the St. St. frequency is enhanced to 58.94 Hz, as shown in Figure 22. Furthermore, as can be shown in Figure 22 (c), the STATCOM controlled by ARO based PD-PIDA provides

TABLE 7. The impact of Gen.2 disconnection on system dynamics with wind farm integration.

Generators	Variables	Without STATCOM	MPA based PIDA STATCOM [35]	ARO-based PD-PIDA STATCOM
Gen.1	Max. U. (Hz)	56.759	58.031	58.21
	St. St. Frequency (Hz)	58.778	58.766	58.94
Gen.3	Max. U. (Hz)	56.771	58.121	58.261
	St. St. Frequency (Hz)	58.751	58.738	58.941
STATCOM	St. St. Q (Mvar)	N/A	127.33	183.22

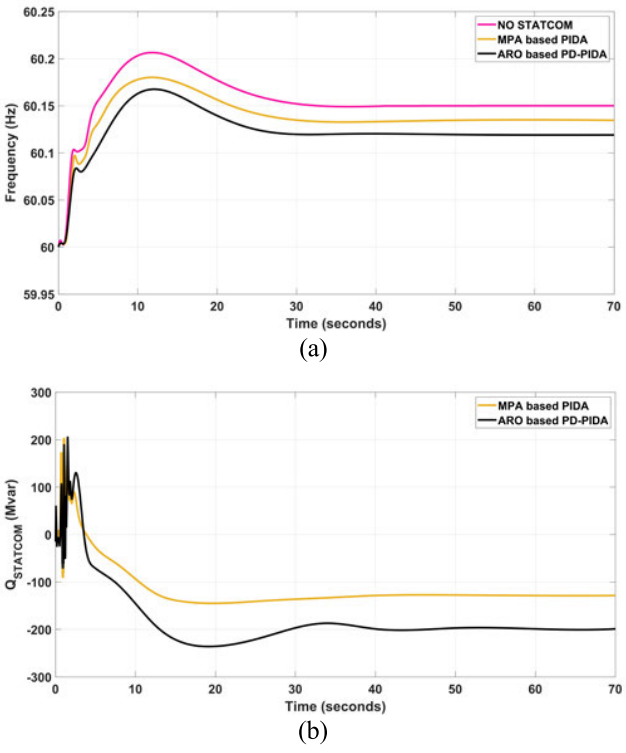

FIGURE 23. The impact of a 20% load loss on IEEE 39 bus system dynamics (a) The system Frequency (b) QSTATCOM.

greater transient inductive power (183.22 Mvar) than the one controlled by the MPA based PIDA. In addition, Table 7 provides a concise summary of the system performance characteristics related to this scenario.

B. THE IEEE 39 BUS SYSTEM CASE STUDY

In a manner analogous to that of the Kundur system, the ARO based PD-PIDA controlled STATCOM performance has been simulated on the IEEE 39 bus system in order to determine whether or not it is capable of enhancing the frequency response of a huge numerous machine system in the face of various disturbances. These disturbances include a loss of 20% of the dynamic load as well as the loss of Gen.4, which is linked with bus 33.

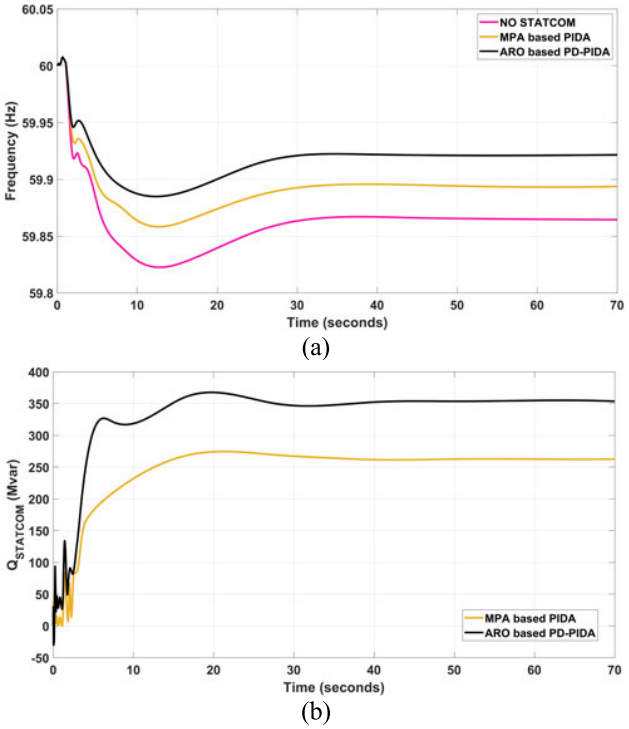

FIGURE 24. The impact of Gen.4 disconnection on IEEE 39 bus system dynamics (a) The system Frequency (b) QSTATCOM.

TABLE 8. The impact of a 20% load loss on ieee 39 bus system dynamics.

	Variables	Without STATCOM	MPA based PIDA STATCOM [33]	ARO-based PD-PIDA STATCOM
Generators	Max. O. (Hz)	60.21	60.18	60.16
	St. St. Frequency (Hz)	60.15	60.135	60.11
STATCOM	St. St. Q (Mvar)	N/A	-129	-201

1) IMPACT OF 20% LOSS IN THE DYNAMIC LOAD

This subsection's objective is to evaluate the resiliency of the provided STATCOM, which is controlled by the ARO-based PD-PIDA. The test will be conducted with the system subjected to a sudden loss of 20% of its load. In Figure 23, the recommended PD-PIDA controller is shown to enhance the Max. O. frequency of the IEEE 39 bus system to 60.16 Hz and the St. St. Frequency to 60.11 Hz, which demonstrates the superiority of the proposed strategy in comparison to the NO STATCOM case and the MPA-based PIDA case. In addition to this, the STATCOM that is handled by the ARO-based PD-PIDA is capable of delivering more transient capacitive power (201 Mvar) than the STATCOM that is handled by the MPA-based PIDA. The system performance characteristics relevant to this situation are listed in a condensed fashion in Table 8.

TABLE 9. The impact of Gen.4 disconnection on ieee 39 bus system dynamics.

	Variables	Without STATCOM	MPA based PIDA STATCOM [33]	ARO-based PD-PIDA STATCOM
Generators	Max. U. (Hz)	59.83	59.86	59.89
	St. St. Frequency (Hz)	59.86	59.89	59.92
STATCOM	St. St. Q (Mvar)	N/A	262	355

2) IMPACT OF GEN.4 DISCONNECTION

In this context, Gen.4, which has been connected to bus 33 of the IEEE 39 bus system, will have its connection to the system terminated. According to the outcomes of the study, the ARO-based PD-PIDA regulator provides a frequency performance that is superior to that offered by the other techniques when placed into comparison. As can be seen in Figure 24 (a), the Max. U. frequency is limited to 59.89 Hz with the assistance of the recommended PD-PIDA controller, and the St. St. frequency has been boosted to 59.92 Hz. In addition, as can be shown in Figure 24 (b), the STATCOM that is controlled by an ARO-based PD-PIDA delivers more transient inductive power (355 Mvar) than the one that is controlled by an MPA-based PIDA. In addition, a succinct description of the system performance characteristics relevant to this situation is included in Table 9.

VII. CONCLUSION

This article offered an inspiring method for controlling frequency that makes use of reactive power modulation and a STATCOM that is controlled by PD-PIDA. The intention is to make use of VAR modulation in order to enhance the frequency performance of power systems in the event that load changes or generation are lost. In order to successfully tune the gains of the recommended PD-PIDA controller, the recently developed bio-inspired meta-heuristic algorithm known as ARO is put to good use. The IEEE's widely used multi-machine test systems (i.e., the two-area four-machine system (Kundur system) and the New England IEEE 39-bus system) are used to evaluate the STATCOM's performance employing ARO-based PD-PIDA control. Comparisons are made between the outcomes of the case studies using the proposed ARO-based PD-PIDA-controlled STATCOM and those using the other controller (i.e., the MPA-based PIDA) provided in the literature. These comparisons reveal that the suggested controller is capable of delivering a superior frequency response. The ARO-based PD-PIDA controller is able to restrict the maximum overshoot (Max. O.) and the steady state frequency (St. St. Frequency) responses to 60.128 Hz and 60.1 Hz, respectively, if the Kundur system is exposed to a load loss of 20%. In addition, the ARO-based PD-PIDA controller is able to restrict the maximum undershoot (Max. U.) and the steady state frequency (St. St. Frequency) responses to 58.89 Hz and 59.32 Hz, respectively, when the Kundur system is exposed to Gen.2 disconnection. On the other hand, The ARO-based PD-PIDA controller is able to restrict the maximum overshoot (Max. O.) and the steady state frequency (St. St. Frequency) responses to 60.16 Hz and 60.11 Hz, respectively, if the IEEE 39 bus system is exposed to a load loss of 20%. In addition, the ARO-based PD-PIDA controller is able to restrict the maximum undershoot (Max. U.) and the steady state frequency (St. St. Frequency) responses to 59.89 Hz and 59.92 Hz, respectively, when the IEEE 39 bus system is exposed to Gen.2 disconnection. Moreover, it has been discovered that the ARO-based PD-PIDA controller is resilient under the effect of wind farm integration into region 2 of the investigated Kundur system. The maximum overshoot (Max. O.) response and the steady state frequency (St. St. Frequency) response for the 20% load loss situation are, respectively, 60.198 Hz and 60.127 Hz. When Gen.2 is not connected, the maximum undershoot (Max. U.) and the steady state frequency (St. St. Frequency) responses are 58.261 Hz and 58.94 Hz, respectively. Also highlighted is the impact that would result from raising the allowable output restrictions of the PD-PIDA regulator to a level that is greater than 5% on the frequency performance of the Kundur system. This technique has the potential to further enhance the frequency performance. In conclusion, the ARO-based PD-PIDA-controlled STATCOM is reliable and has the potential to be successfully utilized to boost the frequency performance of power systems via VAR modulation. In future work, the proposed strategy could be implemented in other standard systems, such as the IEEE 118-bus system, and studies could be conducted for various penetration levels of wind and other renewable sources, such as solar, and a voltage control study could be considered alongside the frequency study.

REFERENCES

[1] N. Hatziargyriou, J. Milanovic, C. Rahmann, V. Ajjarapu, C. Canizares, I. Erlich, D. Hill, I. Hiskens, I. Kamwa, B. Pal, P. Pourbeik, J. Sanchez-Gasca, A. Stankovic, T. Van Cutsem, V. Vittal, and C. Vournas, "Definition and classification of power system stability—Revisited & extended," *IEEE Trans. Power Syst.*, vol. 36, no. 4, pp. 3271–3281, Jul. 2021.

[2] L. Van Dai and L. C. Quyen, *Advanced Solutions in Power System Transient Stability*. Saarland, Germany: LAP Lambert Academic Publishing, 2020.

[3] S. Impram, S. V. Nese, and B. Oral, "Challenges of renewable energy penetration on power system flexibility: A survey," *Energy Strategy Rev.*, vol. 31, Sep. 2020, Art. no. 100539.

[4] J. Shair, H. Li, J. Hu, and X. Xie, "Power system stability issues, classifications and research prospects in the context of high-penetration of renewables and power electronics," *Renew. Sustain. Energy Rev.*, vol. 145, Jul. 2021, Art. no. 111111.

[5] Nahid-Al-Masood, M. N. H. Shazon, S. R. Deeba, and S. R. Modak, "A frequency and voltage stability-based load shedding technique for low inertia power systems," *IEEE Access*, vol. 9, pp. 78947–78961, 2021.

[6] L. Badesa, F. Teng, and G. Strbac, "Conditions for regional frequency stability in power system scheduling—Part II: Application to unit commitment," *IEEE Trans. Power Syst.*, vol. 36, no. 6, pp. 5567–5577, Nov. 2021.

[7] H. Haes Alhelou, M. Hamedani-Golshan, T. Njenda, and P. Siano, "A survey on power system blackout and cascading events: Research motivations and challenges," *Energies*, vol. 12, no. 4, p. 682, Feb. 2019.

[8] N.-A. Masood, M. N. H. Shazon, H. M. Ahmed, and S. R. Deeba, "Mitigation of over-frequency through optimal allocation of BESS in a low-inertia power system," *Energies*, vol. 13, no. 17, p. 4555, Sep. 2020.
[9] J. Atkinson and I. M. Albayati, "Impact of the generation system parameters on the frequency response of the power system: A U.K. grid case study," *Electricity*, vol. 2, no. 2, pp. 143–157, Apr. 2021.
[10] X. Zhao, Y. Xue, and X. Zhang, "Fast frequency support from wind turbine systems by arresting frequency nadir close to settling frequency," *IEEE Open Access J. Power Energy*, vol. 7, pp. 191–202, 2020.
[11] T. Ding, D. Feng, C. Fang, and C. Liu, "Optimal spinning reserve allocation strategy under uncertainties and contingencies," in *Proc. IEEE Power Energy Soc. Gen. Meeting (PESGM)*, Jul. 2016, pp. 1–5.
[12] M. S. Javadi, M. Lotfi, M. Gough, A. E. Nezhad, S. F. Santos, and J. P. S. Catalão, "Optimal spinning reserve allocation in presence of electrical storage and renewable energy sources," in *Proc. IEEE Int. Conf. Environ. Electr. Eng. IEEE Ind. Commercial Power Syst. Eur. (EEEIC/I&CPS Europe)*, Jun. 2019, pp. 1–6.
[13] Nahid-Al-Masood, T. K. Saha, and H. M. Ahmed, "Improving frequency response of a low inertia grid via an appropriate load shedding scheme," in *Proc. IEEE Power Energy Soc. Gen. Meeting (PESGM)*, Aug. 2020, pp. 1–5.
[14] E. Dehghanpour, H. K. Karegar, and R. Kheirollahi, "Under frequency load shedding in inverter based microgrids by using droop characteristic," *IEEE Trans. Power Del.*, vol. 36, no. 2, pp. 1097–1106, Apr. 2021.
[15] J. J. Kim and J. H. Park, "A novel structure of a power system stabilizer for microgrids," *Energies*, vol. 14, no. 4, p. 905, Feb. 2021.
[16] J. H. Chow and J. J. Sanchez-Gasca, *Turbine-Governor Models and Frequency Control, Power System Modeling, Computation, and Control*. Hoboken, NJ, USA: Wiley, 2019, pp. 327–370.
[17] Z. A. Obaid, L. M. Cipcigan, L. Abrahim, and M. T. Muhssin, "Frequency control of future power systems: Reviewing and evaluating challenges and new control methods," *J. Modern Power Syst. Clean Energy*, vol. 7, no. 1, pp. 9–25, Jan. 2019.
[18] A. H. Yakout, M. A. Attia, and H. Kotb, "Marine predator algorithm based cascaded PIDA load frequency controller for electric power systems with wave energy conversion systems," *Alexandria Eng. J.*, vol. 60, no. 4, pp. 4213–4222, Aug. 2021.
[19] Y. A. Dahab, H. Abubakr, and T. H. Mohamed, "Adaptive load frequency control of power systems using electro-search optimization supported by the balloon effect," *IEEE Access*, vol. 8, pp. 7408–7422, 2020.
[20] H. M. Hasanien, "Whale optimisation algorithm for automatic generation control of interconnected modern power systems including renewable energy sources," *IET Gener., Transmiss. Distrib.*, vol. 12, no. 3, pp. 607–614, Feb. 2018.
[21] A. H. Yakout, H. Kotb, H. M. Hasanien, and K. M. Aboras, "Optimal fuzzy PIDF load frequency controller for hybrid microgrid system using marine predator algorithm," *IEEE Access*, vol. 9, pp. 54220–54232, 2021.
[22] A. Fathy, A. M. Kassem, and A. Y. Abdelaziz, "Optimal design of fuzzy PID controller for deregulated LFC of multi-area power system via mine blast algorithm," *Neural Comput. Appl.*, vol. 32, no. 9, pp. 4531–4551, May 2020.
[23] G. Chen, Z. Li, Z. Zhang, and S. Li, "An improved ACO algorithm optimized fuzzy PID controller for load frequency control in multi area interconnected power systems," *IEEE Access*, vol. 8, pp. 6429–6447, 2020.
[24] T. Rahman, M. Kerdphol, and Y. Watanabe, "Optimization of virtual inertia considering system frequency protection scheme," *Electr. Power Syst. Res.*, vol. 170, pp. 294–302, May 2019.
[25] U. Tamrakar, D. Shrestha, M. Maharjan, B. Bhattarai, T. Hansen, and R. Tonkoski, "Virtual inertia: Current trends and future directions," *Appl. Sci.*, vol. 7, no. 7, p. 654, Jun. 2017.
[26] P. González-Inostroza, C. Rahmann, R. Álvarez, J. Haas, W. Nowak, and C. Rehtanz, "The role of fast frequency response of energy storage systems and renewables for ensuring frequency stability in future low-inertia power systems," *Sustainability*, vol. 13, no. 10, p. 5656, May 2021.
[27] P. S. Kundur and O. Malik, *Power System Stability and Control*, 2nd ed. Columbus, OH, USA: McGraw-Hill Education, 2022.
[28] C. Zhao, U. Topcu, N. Li, and S. Low, "Design and stability of load-side primary frequency control in power systems," *IEEE Trans. Autom. Control*, vol. 59, no. 5, pp. 1177–1189, May 2014.
[29] A. Moeini and I. Kamwa, "Analytical concepts for reactive power based primary frequency control in power systems," *IEEE Trans. Power Syst.*, vol. 31, no. 6, pp. 4217–4230, Nov. 2016.
[30] R. K. Varma and E. M. Siavashi, "Enhancement of solar farm connectivity with smart PV inverter PV-STATCOM," *IEEE Trans. Sustain. Energy*, vol. 10, no. 3, pp. 1161–1171, Jul. 2019.
[31] C. Yu, H. Zhou, X. Lu, and J. Lai, "Frequency synchronization and power optimization for microgrids with battery energy storage systems," *IEEE Trans. Control Syst. Technol.*, vol. 29, no. 5, pp. 2247–2254, Sep. 2021.
[32] S. Aminzadeh, M. Tarafdar Hagh, and H. Seyedi, "Reactive power management for microgrid frequency control," *Int. J. Electr. Power Energy Syst.*, vol. 120, Sep. 2020, Art. no. 105959.
[33] K. Stein, M. Tun, M. Matsuura, and R. Rocheleau, "Characterization of a fast battery energy storage system for primary frequency response," *Energies*, vol. 11, no. 12, p. 3358, Dec. 2018.
[34] Z. Akhtar, B. Chaudhuri, and S. Y. R. Hui, "Primary frequency control contribution from smart loads using reactive compensation," *IEEE Trans. Smart Grid*, vol. 6, no. 5, pp. 2356–2365, Sep. 2015.
[35] A. H. Yakout, W. Sabry, A. Y. Abdelaziz, H. M. Hasanien, K. M. AboRas, and H. Kotb, "Enhancement of frequency stability of power systems integrated with wind energy using marine predator algorithm based PIDA controlled STATCOM," *Alexandria Eng. J.*, vol. 61, no. 8, pp. 5851–5867, Aug. 2022.
[36] M. Khudhair, M. Ragab, K. M. AboRas, and N. H. Abbasy, "Robust control of frequency variations for a multi-area power system in smart grid using a newly wild horse optimized combination of PIDD2 and PD controllers," *Sustainability*, vol. 14, no. 13, p. 8223, Jul. 2022.
[37] L. Wang, Q. Cao, Z. Zhang, S. Mirjalili, and W. Zhao, "Artificial rabbits optimization: A new bio-inspired meta-heuristic algorithm for solving engineering optimization problems," *Eng. Appl. Artif. Intell.*, vol. 114, Sep. 2022, Art. no. 105082.
[38] A. E. Khalil, T. A. Boghdady, M. H. Alham, and D. K. Ibrahim, "Enhancing the conventional controllers for load frequency control of isolated microgrids using proposed multi-objective formulation via artificial rabbits optimization algorithm," *IEEE Access*, vol. 11, pp. 3472–3493, 2023.
[39] A. O. Alsaiari, E. B. Moustafa, H. Alhumade, H. Abulkhair, and A. Elsheikh, "A coupled artificial neural network with artificial rabbits optimizer for predicting water productivity of different designs of solar stills," *Adv. Eng. Softw.*, vol. 175, Jan. 2023, Art. no. 103315.
[40] V. Janamala, K. Radha Rani, P. Sobha Rani, A. N. Venkateswarlu, and S. R. Inkollu, "Optimal switching operations of soft open points in active distribution network for handling variable penetration of photovoltaic and electric vehicles using artificial rabbits optimization," *Process Integr. Optim. Sustainability*, vol. 7, nos. 1–2, pp. 419–437, Mar. 2023.
[41] A. Dixon, *Modern Aspects of Power System Frequency Stability and Control*. San Diego, CA, USA: Academic, 2019.
[42] T. Athay, R. Podmore, and S. Virmani, "A practical method for the direct analysis of transient stability," *IEEE Trans. Power App. Syst.*, vol. PAS-98, no. 2, pp. 573–584, Mar. 1979.
[43] J. Sanam, S. Ganguly, and A. K. Panda, "Distribution STATCOM with optimal phase angle injection model for reactive power compensation of radial distribution networks," *Int. J. Numer. Model., Electron. Netw., Devices Fields*, vol. 30, no. 6, p. e2240, Nov. 2017.
[44] S. Boyd and L. Vandenberghe, *Convex Optimization*. Cambridge, U.K.: Cambridge Univ. Press, 2016.
[45] *In the City, Rabbits Build More Densely*. Pinterest. Accessed: Jan. 31, 2023. [Online]. Available: https://ar.pinterest.com/pin/463659724117065442/
[46] A. Faramarzi, M. Heidarinejad, S. Mirjalili, and A. H. Gandomi, "Marine predators algorithm: A nature-inspired metaheuristic," *Exp. Syst. Appl.*, vol. 152, Aug. 2020, Art. no. 113377.
[47] M. Dehghani, E. Trojovská, and P. Trojovský, "A new human-based metaheuristic algorithm for solving optimization problems on the base of simulation of driving training process," *Sci. Rep.*, vol. 12, no. 1, p. 9924, Jun. 2022.

NABEEL MOHAMMED NEAMAH received the B.Sc. degree in electrical engineering from the Faculty of Engineering, Diyala University, Diyala, Iraq, in 2015. He is currently an Engineer in electrical maintenance with Diyala University. His current research interests include power management, power system control, modern control techniques, renewable energy sources, and power quality issues.

AHMED ABUHUSSEIN (Member, IEEE) received the B.S. degree in electrical power engineering from Tafila Technical University (TTU), Tafila, Jordan, and the M.S. and Ph.D. degrees in ECE from The University of Memphis, Tennessee, USA. He is currently an Assistant Professor with the Department of Electrical and Computer Engineering (ECE), Gannon University. His research interests include fault current limiters, power quality, geomagnetically induced currents (GIC), power electronics, electrical machines, AC/DC microgrids, renewable energy systems, energy storage systems, and flexible AC transmission systems (FACTS).

AHMED A. HOSSAM-ELDIN (Life Senior Member, IEEE) received the B.Sc. (Hons.) and M.Sc. degrees in electrical engineering from Alexandria University, Egypt, in 1965 and 1969, respectively, and the Ph.D. degree in electrical and electronic engineering from Heriot-Watt University, Edinburgh, U.K., in 1972. He has been a Professor in electrical materials and power engineering, since 1983. He is the electrical, energy and environmental consultant for 160 governmental and private projects. He was the Consultant of the Social Development Fund (SDF). He is registered as an Expert in Water Desalination Using Renewable Energy for the UNESCO 2004. He is globally recognized for his academic achievements and overall leadership contributions to his society and the world. He has published 325 papers in international journals and conferences. He is the author of five international books in HV engineering, electrical materials, electric circuits, and instrumentation and logic circuits. His biography was published in the Encyclopaedia of the Best Egyptian Figures, in 1979, ''Who is Who'' of Engineering ''Who is Who'' of the world and in Britain. He patented some of his work. He supervised 181 postgraduate students for the M.Sc. and Ph.D. degrees. He is the principal investigator (PI) for 40 research projects. He was a visiting professor to many universities worldwide. He participated and chaired many international conferences. He is a Life Senior Member of the IET, CIGRE, WEC, Institute of Physics, and the New York Academy of Science. He is a member of many committees in universities, ministries, and governorates. He is an Executive Member of the Engineering Sector Committee for Higher Education Strategy (SCU) and the X-Chairperson of the Promotion Committee for Professors and Associates (SCU). He is a Technical Advisor to Chairperson of Arab Organization of Industrialization (AOI), an Executive Member of the Electricity Board of the Egyptian Electrical Transmission Company, and a member of the General Assembly of the Ministry of Electricity. He received many outstanding international, top national awards, and golden medals presented personally to him in a special ceremony by The Presidents of Egypt. In 1993, he received the Certificate of Honour from the New York Academy of Sciences for his Distinguished Scientific Work and Achievements for the benefit of his society. He has been awarded (twice) by the Egyptian Council of Professional Engineers Golden Medal. He received the IEEE Award for Best Paper, in 1976. He is the Chairperson of the Engineering Committee for Top National Awards (ASRT). He is a reviewer and an editor of many international journals.

SULTAN ALGHAMDI (Member, IEEE) received the Ph.D. degree in electrical engineering from the University of Leeds, U.K., in 2020. Currently, he is an Assistant Professor with the Department of Electrical and Computer Engineering, King Abdulaziz University, Jeddah, Saudi Arabia. His current research interests include distributed control and time-delay systems with application to microgrids and power systems.

KAREEM M. ABORAS received the B.Sc., M.Sc., and Ph.D. degrees in electrical engineering from the Faculty of Engineering, Alexandria University, Alexandria, Egypt, in 2010, 2015, and 2019, respectively. His Ph.D. research work is focused on the performance enhancement of renewable energy conversion systems. Currently, he is an Assistant Professor with the Electrical Power and Machines Department, Faculty of Engineering, Alexandria University. He is a reviewer for IEEE TRANSACTIONS ON ENERGY CONVERSION, *Smart Science*, *Alexandria Engineering Journal*, *IET*, *Energy Reports*, IEEE ACCESS, *Cybernetics and Systems*, *Protection and Control of Modern Power Systems*, MDPI, *Journal of Advanced Research in Applied Sciences and Engineering Technology*, *Cogent Engineering*, and Hindawi journals. His research interests include power electronics, control, drives, power systems, smart grids, microgrids, power quality, optimizations, electric vehicles, machine learning, modeling, fuel cells, HVDC, and renewable energy systems.